

Prospects for Probing the Three Gauge-boson Couplings in $W + \text{Photon}$ Production at the LHC

Matt Dobbs* and Michel Lefebvre†

*Department of Physics and Astronomy, University of Victoria,
P.O. Box 3055, Victoria, British Columbia, Canada V8W 3P6*

(Dated: September 16, 2002)

We assess the prospects for probing the $WW\gamma$ triple gauge-boson coupling directly by means of hadronic $W\gamma$ production at the 14 TeV Large Hadron Collider (LHC) using the ATLAS detector. The expected confidence intervals for anomalous couplings are presented including the effects of higher order QCD corrections and the contributions from systematic effects. A strategy for reporting the anomalous couplings limits is introduced which removes the ambiguities of form factors, by reporting the limits as a function of a cutoff operating on the diboson system invariant mass. Techniques for measuring the energy dependence of anomalous couplings are demonstrated.

Contents

I. Introduction	2
II. Phenomenology	3
A. Effective Three Gauge-boson Lagrangian	3
B. Radiation Zero	5
C. Higher Order Corrections	6
D. Unitarity Limits and Form Factors	7
E. Current Limits on Anomalous $WW\gamma$ Couplings	8
III. Detector and Physics Simulation	9
A. Signal Simulation	9
B. Background Simulation	10
C. Detector Simulation	11
D. Particle Identification in ATLAS	12
IV. Backgrounds and Event Selection	13
A. Backgrounds with a Lepton and Photon Signature	13
B. Jets Mis-identified as Electrons	15
C. Jets Mis-identified as Photons	15
D. Event Selection and Efficiency	16
V. Analysis Methods and Results	19
A. Observing the Radiation Zero at LHC	19
B. Methods for Measuring Anomalous Coupling Parameters	21
C. Systematic Uncertainties	26

*Electronic address: matt.dobbs@cern.ch

†Electronic address: lefebvre@uvic.ca

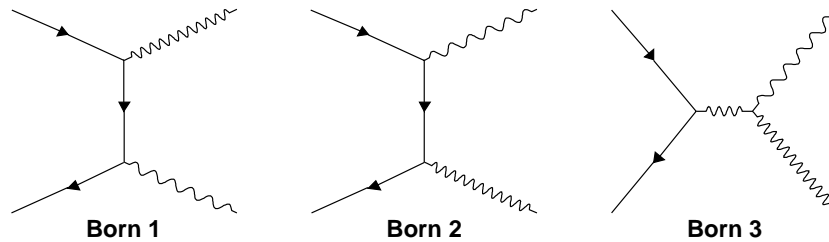


FIG. 1: The Born-level Feynman graphs for $q\bar{q}' \rightarrow W\gamma$. The s -channel diagram (right) contains a TGC vertex, whereas the t -channel diagrams (left and middle) do not.

D. Results and Comparison of Methods	30
E. Controlling Systematics	34
F. Limits as a Function of Integrated Luminosity	36
G. Limits as a Function of Form Factor Scale and Mass Scale	40
H. Measuring the Energy Dependence of Anomalous TGC's	43
VI. Conclusions	44
Acknowledgements	45
References	45
Appendix	47
Event Reweighting as a Function of Anomalous Couplings	47
Reconstructing the Centre-of-Mass System Kinematics	49

I. INTRODUCTION

In the Standard Model (SM), the gauge-bosons interact not only with matter particles, but also with one another. These interactions manifest themselves as a coupling between three (or more) gauge-bosons, such as a WWZ or $WW\gamma$ coupling, referred to as triple gauge-boson couplings (TGC's). The existence of these couplings has been beautifully verified at the Large Electron Positron collider (LEP) [1–4]. TGC's are tightly connected with the symmetry properties of the model and reflect the full mathematical gauge group structure of the fundamental interactions. The production of gauge-boson pairs in hadronic collisions is sensitive to triple gauge-boson couplings, providing a direct test of these interactions. Any deviation from the SM prediction would indicate the presence of new physics.

The TGC interactions are often referred to as 'self-couplings', because they involve interactions between gauge-bosons. The simplest manifestation of these gauge-boson self-couplings is the WWZ and $WW\gamma$ interaction vertices. ZZZ , $ZZ\gamma$, $Z\gamma\gamma$, and $\gamma\gamma\gamma$ vertices are not allowed in the model, because neither the Z nor the γ carries charge or weak isospin which are the quantum numbers to which the gauge-bosons couple. Vertices containing an odd number of W -bosons (WZZ , $W\gamma\gamma$, $WZ\gamma$, WWW) are excluded by charge conservation. The self interactions also encompass interactions between four gauge-boson (quartic couplings).

This paper focuses on the prospects of measuring anomalous contributions to the $WW\gamma$ coupling through $pp \rightarrow W^\pm\gamma \rightarrow l^\pm\nu\gamma$ (where l is an electron or muon) production at the LHC

with the ATLAS detector. Three Feynman graphs contribute to hadronic $W^\pm\gamma$ production at leading order, as shown in Figure 1. Of these three diagrams, only the s -channel diagram contains a triple gauge-boson coupling.

The study presented in this paper is optimized for “low luminosity” ($10^{33}\text{cm}^{-2}\text{s}^{-1}$) LHC conditions. It extends the leading order studies of the charged anomalous TGC’s in the context of ATLAS which appear in Refs.[5, 6]. This $W\gamma$ study complements the study of the WZ channel which appears in Ref. [7]. Refs. [8] address the prospects for measuring the neutral TGC couplings in the ZZ and $Z\gamma$ channels with ATLAS.

The structure of this paper is as follows. The phenomenology of diboson production is discussed in the next section. The software chain which has been used to simulate the physics processes and detector are reviewed in Section III. Backgrounds and the kinematic cuts which are used to isolate the signal are presented in Section IV. Several methods for measuring the TGC vertex are described, evaluated, and compared in Section V before summarising the study in the concluding section.

II. PHENOMENOLOGY

A. Effective Three Gauge-boson Lagrangian

The Standard Model $WW\gamma$ vertex is uniquely determined by requiring $SU(2)_L \times U(1)_Y$ gauge invariance to be valid at arbitrary energy scales. Deviation from the SM vertex (i.e. anomalous couplings) would signal new physics, which could arise from loop corrections involving propagators of new particles or from unexpected internal structure of the particles which are believed to be fundamental (e.g. composite gauge-bosons). Assuming the new physics occurs at an energy scale significantly larger than that being probed experimentally, it can be integrated out, and expressed as a set of anomalous interaction vertices. As such, experimental attempts to measure anomalous TGC parameters probe the low energy remnants of new physics which may be operating at a much higher energy scale. Measurements of this type would be most interesting in the scenario where direct searches for new particles which affect the gauge-boson interactions fail to observe any substantial deviation from the SM.

The most general Lorentz and gauge invariant anomalous $WW\gamma$ TGC vertex is described by 4 parameters (ignoring any theoretical or experimental constraints) and may be written in terms of an effective Lagrangian [9–11]

$$\begin{aligned}
i\mathcal{L}^{WW\gamma}/g_{WW\gamma} &= A^\mu(W_{\mu\nu}^-W^{+\nu} - W_{\mu\nu}^+W^{-\nu}) \\
&+ (1 + \Delta\kappa_\gamma)W_\mu^+W_\nu^-F^{\mu\nu} + \frac{\lambda_\gamma}{M_W^2}F^{\mu\nu}W_\nu^{+\rho}W_{\rho\mu}^- \\
&- \frac{\tilde{\kappa}_\gamma}{2}W_\mu^-W_\nu^+\varepsilon^{\mu\nu\rho\sigma}F_{\rho\sigma} - \frac{\tilde{\lambda}_\gamma}{2M_W^2}W_{\rho\mu}^-W_\nu^{+\mu}\varepsilon^{\nu\rho\alpha\beta}F_{\alpha\beta}
\end{aligned} \tag{1}$$

where M_W is the W -boson mass, A^μ and W^μ are the photon and W fields, $W_{\mu\nu} = \partial_\mu W_\nu - \partial_\nu W_\mu$, and $F_{\mu\nu} = \partial_\mu A_\nu - \partial_\nu A_\mu$. The normalisation factor is chosen for convenience to be $g_{WW\gamma} = -e$.

There are four anomalous $WW\gamma$ parameters (referred to here as anomalous TGC’s) in

total.¹ Strictly speaking, these parameters may be energy dependent. This will be discussed in Section II D. As they are written in Equation 1, all anomalous TGC's are zero in the SM.

The operators in the Lagrangian with coefficients $\tilde{\kappa}_\gamma$ and $\tilde{\lambda}_\gamma$ are odd under parity (P) transformations and even under charge (C) transformations, meaning they violate CP. For simplicity, we assume CP conservation. This reduces the number of anomalous TGC's for the $WW\gamma$ vertex to two: $\Delta\kappa_\gamma$ and λ_γ .

In order to better understand how the effective Lagrangian relates to kinematic variables, the approximate modifications to the matrix element amplitudes are presented here. In the high energy limit ($\hat{s} \gg M_W^2$, where $\sqrt{\hat{s}}$ is the parton centre of mass energy) the change in the matrix element $\Delta\mathcal{M}_{H_\gamma, H_W}$ arising from anomalous TGC's for the leading order partonic process $q\bar{q}' \rightarrow W\gamma$ is [11, 12]

$$\Delta\mathcal{M}_{\pm,0} \propto \frac{\sqrt{\hat{s}}}{2M_W} [\Delta\kappa_\gamma + \lambda_\gamma] \frac{1}{2} (1 \mp \cos\theta_\gamma^*), \quad (2)$$

$$\Delta\mathcal{M}_{\pm,\pm} \propto \left[\frac{\hat{s}}{2M_W^2} \lambda_\gamma + \frac{1}{2} \Delta\kappa_\gamma \right] \frac{1}{\sqrt{2}} \sin\theta_\gamma^*, \quad (3)$$

where H_W, H_γ are the W, γ helicities and $\sin\theta_\gamma^*$ is the production angle of the photon with respect to the quark direction in the parton centre of mass frame. The CP violating anomalous TGC's have been omitted to simplify the equations. A zero helicity photon ($H_\gamma = 0$) is not allowed because the photon is massless.

The first thing to notice from Eqs. 2 and 3 is the importance of the dimensionality of the operators in the Lagrangian. The $\Delta\kappa_\gamma$ coupling is the coefficients of a dimension four operator, and its enhancement is proportional only to $\sqrt{\hat{s}}$. The λ_γ coupling is the coefficient of a dimension six operator and it enhances the cross section by a factor proportional to the parton centre of mass energy squared \hat{s} . Because of this energy squared enhancement, the sensitivity to the λ_γ coupling increases rapidly with increased collider energy. This will provide a distinct advantage for the 14 TeV LHC collider as compared to the 2 TeV Tevatron collider.

Another important factor is the angular term in Eqs. 2 and 3. The λ_γ coupling enjoys an enhancement proportional to $\sin\theta_\gamma^*$, which means the effect will be largest in the direction transverse to the quark direction (i.e. transverse to the beam). This corresponds to the central part of a particle detector, where the best measurements are possible. This too, will provide an advantage when probing the λ_γ coupling as compared to $\Delta\kappa_\gamma$.

From the approximate matrix element modifications, it can be seen that several experimental observables can be used to extract information about the anomalous TGC parameters from an ensemble of diboson events: (1) Event Rate: The cross section, which is proportional to the matrix element squared, is sensitive to the modified matrix elements. (2) Energy Behaviour: The effect of anomalous TGC's increases with diboson invariant mass, meaning non-standard couplings would enhance the cross section most at high parton centre of mass energy. (3) Production Angle: The contribution from the anomalous TGC's depends on the gauge-boson production angle (polar angle with respect to the beam). Since the SM cross section is suppressed in the region of the radiation zero (see Section II B), this effect will be of particular importance in the central regions. (4) Polarisation: The gauge-boson helicity has a direct effect on the boson decay angles, which means that the angular distributions (and transverse

¹ This differs from the case of the WWZ vertex, for which there are an additional 3 parameters: $\Delta g^1, g^4$, and g^5 . For on-shell photons in the final state, these additional parameters are absent since g^4 and g^5 are proportional to p_γ^2 and since electromagnetic gauge invariance requires $\Delta g^1 = 0$ for on-shell photons.

momentum) of the boson decay products can be used to project out specific helicity states. In Section V, various techniques for exploiting this information will be explored.

B. Radiation Zero

The Born level SM differential cross section for $d\bar{u} \rightarrow W^- \gamma$ is [13]

$$\frac{d\hat{\sigma}^{\text{SM}}}{d\cos\theta_{\bar{q},\gamma^*}} = \text{CONST} \times \frac{1}{\hat{s}(1 - \frac{M_W^2}{\hat{s}})} \frac{(\cos\theta_{\bar{q},\gamma^*} + 1/3)^2 \left[(1 + \frac{M_W^2}{\hat{s}})^2 + (1 - \frac{M_W^2}{\hat{s}})^2 \cos^2\theta_{\bar{q},\gamma^*} \right]}{1 - \cos^2\theta_{\bar{q},\gamma^*}}, \quad (4)$$

where CONST is an unimportant overall factor, $\cos\theta_{\bar{q},\gamma^*}$ is the scattering angle of the photon relative to the incoming antiquark in the $q\bar{q}$ centre-of-mass frame, and \hat{s} is the centre-of-mass energy squared. The *radiation zero* refers to the cancellation which occurs at $\cos\theta_{\bar{q},\gamma^*} = -1/3$ for $W^- \gamma$ production ($\cos\theta_{\bar{q},\gamma^*} = 1/3$ for $W^+ \gamma$). An approximate radiation zero exists for $W^\pm Z^0$ production as well, for which more details can be found in Ref. [14].

At the present time, the radiation zero has yet to be observed experimentally. The prospects for observing it at the Tevatron from Run II data are good [15, Sec. 4.6.1].

For hadronic collisions, it is not possible to ascertain from which beam the quark or antiquark arises. This makes the distribution for $\cos\theta_{\bar{q},\gamma^*}$ impossible to observe experimentally. Instead, one may reconstruct the centre-of-mass production angle $\cos\theta_{\gamma^*}$ of the γ with respect to one of the beams. The symmetric proton-proton beams imply that the distribution is also symmetric, and so the effect of the radiation zero is a dip at $\cos\theta_{\gamma^*} = 0$, rather than a cancellation at $\cos\theta_{\bar{q},\gamma^*} = \pm 1/3$. At a $p\bar{p}$ collider such as the Tevatron, the quark is statistically most likely to arise from the proton beam valence quark distributions, while the antiquark will most often arise from the antiproton valence distributions, and so an antisymmetric distribution persists, though the sea quark contribution to the (anti)proton washes out the effect somewhat.

Anomalous couplings spoil the radiation zero cancellations. For most choices of the anomalous TGC parameters, this results in a ‘filling in’ of the radiation zero dip.

There are complications with reconstructing the centre-of-mass frame for processes with a neutrino in the final state, as is the case for the leptonic decays in $W\gamma$ production, because the longitudinal momentum of the neutrino is not measured experimentally (this will be discussed in more detail in the appendix). The rapidity separation of the photon from the charged lepton arising in the W^\pm decay ($\eta_\gamma - \eta_{\frac{\pm}{W}}$) is a distribution which can be reconstructed without knowing the neutrino four-momentum, and is sensitive to the radiation zero. Like the $\cos\theta_{\gamma^*}$ distribution, the $(\eta_\gamma - \eta_{\frac{\pm}{W}})$ distribution is symmetric for pp collisions with a dip at $(\eta_\gamma - \eta_{\frac{\pm}{W}}) = 0$. For $p\bar{p}$ collisions the dip is slightly off-centre, providing the characteristic signature of the radiation zero.

In terms of the radiation zero asymmetry being masked by symmetric beams, a similar situation exists for measurements of the forward-backward asymmetry in $pp \rightarrow Z^0/\gamma^* + X \rightarrow l^+l^- + X$ production. The asymmetry exists in the production angle of the Z^0/γ^* with respect to the incoming quark direction, but the two beams are symmetric and so no asymmetry exists with respect to the beams. However, in Refs. [16, 17], the idea of ‘signing’ the forward direction according to the direction (or boost) of the Z^0/γ^* in the laboratory frame is presented. Valence quarks inside the proton normally have a larger momentum fraction than sea quarks. Because the quark which participates in the reaction will predominantly come from the valence distribution in the proton, whereas the antiquark will always come from the sea distribution,

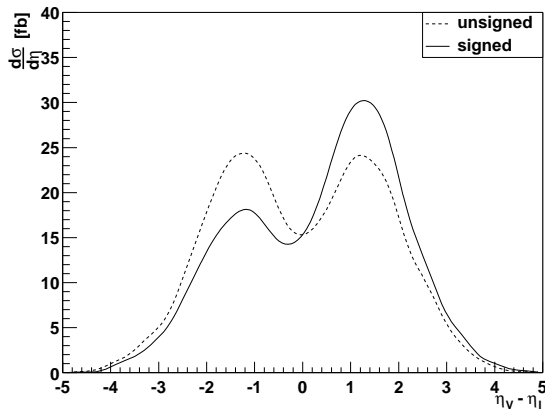


FIG. 2: The rapidity separation of the γ from the l_W^\pm is shown for $W\gamma$ production at the LHC. For the solid lines, the rapidity separation has been ‘signed’ according to Eq. 5. The distributions are generated at NLO using the parton level generator of Ref. [18] (hadronization and detector effects are not included). The kinematic cuts are chosen to coincide with the present analysis, with the exception of the cut on the jet transverse momentum, which is set to 30 GeV for this figure.

the Z^0 will usually be boosted in the quark direction of travel. This provides a statistical means of ‘signing’ the forward direction for this process.

This idea is applied to diboson production for the first time here. The longitudinal momentum of the γ , l_W^\pm system $P_{\gamma, l_W^\pm}^z$ is evaluated. If the longitudinal momentum is in the forward direction ($P_{\gamma, l_W^\pm}^z > 0$), the rapidity separation is not altered. If it is in the backwards direction ($P_{\gamma, l_W^\pm}^z < 0$), the sign of the rapidity separation is reversed $\eta_\gamma - \eta_{l_W^\pm} \rightarrow -\eta_\gamma + \eta_{l_W^\pm}$. To account for the difference in the location of the radiation zero for $W^+\gamma$ vs. $W^-\gamma$ production, the sign of the rapidity separation is also reversed when the charged lepton from the W^\pm decay has a negative charge. The signed rapidity separation variable is thus

$$\text{Signed Rapidity Separation} = \text{sign}(Q_{l_W^\pm}, 1) \times \text{sign}(P_{\gamma, l_W^\pm}^z, 1) \times (\eta_\gamma - \eta_{l_W^\pm}), \quad (5)$$

where the $\text{sign}(a, b)$ operator transfers the sign of a on to b . The signed rapidity separation distribution for $W^\pm\gamma$ production is compared to the unsigned distribution in Figure 2 for 14 TeV pp collisions at the LHC. It allows for the observation of the characteristic asymmetric rapidity separation at a pp collider.

C. Higher Order Corrections

Next-to-leading order (NLO) QCD corrections to $W\gamma$ diboson production are large at LHC energies, particularly in the physically interesting region of high transverse momentum which is the same region of maximum sensitivity to anomalous TGC’s. NLO QCD corrections typically increase the inclusive LHC diboson production cross section by about 30% [18]. In the high transverse momentum region, QCD corrections can increase the differential cross section by a factor 2-10. For $W\gamma$ production, the radiation zero suppresses the Born contribution and NLO corrections are even larger [18] than for other diboson processes like WW , ZZ , and $Z\gamma$ production which do not exhibit radiation zeros. Since the $O(\alpha_s)$ subprocesses responsible for the enhancement at large transverse momentum do not involve the three gauge-boson vertex, the overall effect of NLO corrections is a spoiling of sensitivity to anomalous TGC’s.

Rejecting events with hard jets in the central rapidity region (referred to as a *jet veto*), serves to recover anomalous TGC sensitivity which is otherwise lost when introducing NLO corrections. Ref. [19] reports a 10-30% improvement in anomalous TGC sensitivity limits in WZ production when a jet veto is applied as compared to the inclusive NLO case, making the

limits close to those obtained from leading order (LO) distributions. For this analysis, wherein NLO effects will be studied and taken into account, the jet veto strategy will be used.

D. Unitarity Limits and Form Factors

Anomalous TGC's spoil the gauge structure of the model. Departure from this structure can violate unitarity at relatively low energies² and so it has become standard to introduce protection in the effective Lagrangian for triple gauge-boson vertices by expressing the anomalous couplings as scale dependent form factors, which are suppressed at high energy. In this paper we will introduce a different philosophy for ensuring unitarity. We advocate reporting the anomalous TGC measurements as a function of an invariant mass cutoff applied to the data, rather than introducing an arbitrary form factor into the model. In this section, the traditional form factor treatment is reviewed and the diboson mass cutoff philosophy is introduced.

Unambiguous and model-independent constant unitarity constraints for $W\gamma$ production have been derived³ in Ref. [20],

$$\Lambda^2 = 0.99 \text{ TeV}^2 / |\lambda_\gamma| \qquad \Lambda^2 = 1.86 \text{ TeV}^2 / |\Delta\kappa_\gamma| \qquad (6)$$

where Λ is the scale at which unitarity is violated if constant anomalous TGC's are introduced in the Lagrangian.

To conserve unitarity at arbitrary energies it is traditional to introduce the anomalous TGC's as form factors. Thus, for example, the λ_γ anomalous parameter becomes $\lambda_\gamma = \lambda_{\gamma_0} \times \mathcal{F}(q_1^2, q_2^2, P^2)$ and vanishes when q_1^2 , q_2^2 , or P^2 becomes large, where q_1^2 and q_2^2 are the invariant masses squared of the final state bosons and $P^2 = M_{W\gamma}^2$ is the virtual exchange boson invariant mass squared. λ_{γ_0} is referred to as the ‘‘bare coupling’’ and λ_γ is the anomalous TGC form factor which appears in the Eq. 1 Lagrangian. For diboson production the final state bosons are nearly on-shell $q_1^2 = 0$ and $q_2^2 \simeq M_W^2$ even when finite width effects are taken into account. However, large (potentially unitarity violating) virtual exchange boson masses $M_{W\gamma}$ will be probed at the LHC.

The choice of parametrisation for the form factors is arbitrary provided unitarity is conserved at all energies for a sufficiently small value of anomalous coupling. Most common in the literature is a generalised dipole form factor⁴

$$\lambda_\gamma = \frac{\lambda_{\gamma_0}}{\left(1 + \frac{M_{W\gamma}^2}{\Lambda_{\text{FF}}^2}\right)^n} \qquad \Delta\kappa_\gamma = \frac{\Delta\kappa_{\gamma_0}}{\left(1 + \frac{M_{W\gamma}^2}{\Lambda_{\text{FF}}^2}\right)^n} \qquad (7)$$

where $n > 1/2$ is sufficient for the $\Delta\kappa_\gamma$ coupling and $n > 1$ is sufficient for the λ_γ coupling. It is conventional [18, 19, 21] to use $n = 2$ for all of the $WW\gamma$ vertex anomalous TGC's. Unitarity limits for generalised dipole form factors are [12]

$$|\lambda_\gamma| \leq \frac{n^n}{(n-1)^{n-1}} \frac{0.96 \text{ TeV}^2}{\Lambda_{\text{FF}}^2} \qquad |\Delta\kappa_\gamma| \leq \frac{n^n}{(n-1)^{n-1}} \frac{1.81 \text{ TeV}^2}{\Lambda_{\text{FF}}^2} \qquad (8)$$

² In other words, the SM Lagrangian is the only description of the three gauge-boson vertex which is valid up to arbitrary energy scales.

³ Cancellations may occur if more than one anomalous coupling is allowed non-zero at a time, which weakens the unitarity limits somewhat.

⁴ At leading order $M_{W\gamma}^2 = \hat{s}$, which is the notation commonly used in the literature.

For an $n = 2$ dipole form factor with scale $\Lambda_{\text{FF}} = 10$ TeV, this translates to unitarity limits of

$$|\lambda_\gamma| \leq 0.038 \qquad |\Delta\kappa_\gamma| \leq 0.072. \qquad (9)$$

For the present analysis, a constant form factor has been used. This is equivalent to $\Lambda_{\text{FF}} = \infty$, and is unitarity violating at high energy. By using constant form factors, the analysis is free of arbitrary form factor assumptions, and thus can provide the most robust, informative limits. However, the limits will be better than would be obtained with a form factor, so limits as a function of the dipole form factor scale Λ_{FF} will also be presented, such that the limits without an energy dependent form factor can be translated to expectations for other form factor assumptions.

Since the parametrisation of energy dependent form factors is arbitrary and introduces unnecessary dependence on the parametrisation choice into the experimental results, a different strategy is advocated here. Rather than introduce protection against unitarity violating couplings into the Lagrangian, the results will be presented as a function of a diboson invariant mass cutoff which is applied to the data. This makes the behaviour of the limits as a function of invariant mass apparent, provides generic information about the scale to which the experiment is sensitive, and allows for interpretations of the results at different mass scales. If the limits fall outside of the unitarity bounds, then the scale at which this occurs will be clear, and the limits can be evolved back to any mass scale. Limits of this form will be demonstrated in Sec. V G.

ATLAS is sensitive to diboson mass scales up to about 3 TeV, which translates to dipole form factor scales of about 5-10 TeV. It will be shown that the limits for the $WW\gamma$ TGC parameters attainable at ATLAS will be at a level that are below the unitarity constraints at the scales to which the data is sensitive.

E. Current Limits on Anomalous $WW\gamma$ Couplings

The four LEP experiments ALEPH, DELPHI, L3, and OPAL have searched for anomalous TGC's and achieved the most stringent direct experimental limits to date. The most recent combination of the results from the four experiments is presented in Ref. [22], but includes only the data up to the end of 1999 at a centre-of-mass energy up to 202 GeV (i.e. does not yet include all of the data from LEP 2). The limits are derived from W -pair production ($e^+e^- \rightarrow W^+W^-$), single W -production ($W e\nu$), and single photon production ($\gamma\nu\bar{\nu}$), and are sensitive to anomalous couplings in both the WWZ and $WW\gamma$ vertex. The LEP combined 95% confidence intervals

$$\begin{aligned} -0.089 < \lambda_\gamma < 0.20, \\ -0.13 < \Delta\kappa_\gamma < 0.13 \end{aligned} \qquad (10)$$

are derived assuming the contribution to the λ -type couplings from the WWZ and $WW\gamma$ vertices are equal ($\lambda_\gamma = \lambda_Z$), and that the κ -type coupling in the WWZ vertex is related to the $WW\gamma$ coupling by $\Delta\kappa_Z = \Delta g_Z^1 - \Delta\kappa_\gamma \tan^2 \theta_W$, where Δg_Z^1 is an additional anomalous coupling allowed in the WWZ vertex only.

The expected limits for Run II at the 2 TeV $p\bar{p}$ Tevatron collider have been assessed in Ref. [15], assuming an integrated luminosity of 2 fb^{-1} , and are similar to the limits already obtained at LEP.

III. DETECTOR AND PHYSICS SIMULATION

This section focuses on the Monte Carlo programs which have been used to simulate the signal and backgrounds. We also review the particle identification capabilities of the ATLAS detector, which are particularly important for TGC studies.

A. Signal Simulation

Several Monte Carlo programs for hadronic diboson event simulation are in common use. General purpose showering and hadronization event generators (SHG's) such as `PYTHIA` [Sjö01b] evaluate the matrix element at leading order and use the parton shower approach to include higher order corrections—but limited or no anomalous couplings are included.

Programs have been implemented to calculate diboson production with leptonic decays to next-to-leading order (NLO) in QCD. The importance of including the NLO matrix elements in TGC studies has already been discussed in Sec. II C, where it was shown that NLO corrections have the largest effect in the region of high transverse momentum gauge-bosons—the same region which provides maximal sensitivity to anomalous TGC's. This is also the region where the parton shower approach does a poor job of approximating higher order corrections, and so the use of NLO programs is mandatory for an accurate description of the physics.

The NLO diboson generator by Baur, Han, and Ohnemus [18] (BHO) has been used to simulate the signal in this paper. It is based on the programs of Ref. [23] and employs the 2 parameter phase space slicing method [24, 25] in the narrow width approximation. Anomalous TGC's are included. Spin correlations in the leptonic decays are accounted for everywhere except in the virtual contribution. The authors expect a negligible overall effect from neglecting the spin correlations in the virtual corrections as compared to the uncertainty from parton distribution functions and the choice of factorisation scale.⁵

NLO programs like the BHO generator are capable of producing weighted events only. As such, a large number of weighted events need to be produced in order to effect the cancellations which are inherent in the NLO programs. In order to avoid spending a large fraction of the computational time processing events which will later fail the selection criteria, a number of parton level cuts are imposed. The parton level cuts are chosen to be sufficiently far from the final selection cuts such that the detector simulation is unable to smear the events such that they pass the selection.

At NLO the final state consists of the gauge-bosons (or their leptonic decay products) and at most one coloured parton. Before these events can be simulated in the detector environment, final state coloured partons need to be converted into colour-singlet composite hadrons. For the events with a coloured parton in the final state, the method of *independent fragmentation* is used (see e.g. section 5.6.1 of Ref. [27] for a description), followed by hadronization, to produce the colour-singlet particles which form the input to the detector simulation. The `PYTHIA 6.136` [28] program is used for independent fragmentation and hadronization. The standard parton shower approach cannot be applied to the events produced by the BHO generator, because this would double count regions of phase space.

⁵ This has been verified in Ref. [26], wherein the predictions of the BHO WZ and WW generators are compared to those of the DKS generators, which include the full correlations. The original comparison showed an $\mathcal{O}(3\%)$ discrepancy in the WW predictions. Since then, a small error was discovered and corrected in the BHO WW program (for details see Ref. [15, p.152]), and the two programs are now in good agreement.

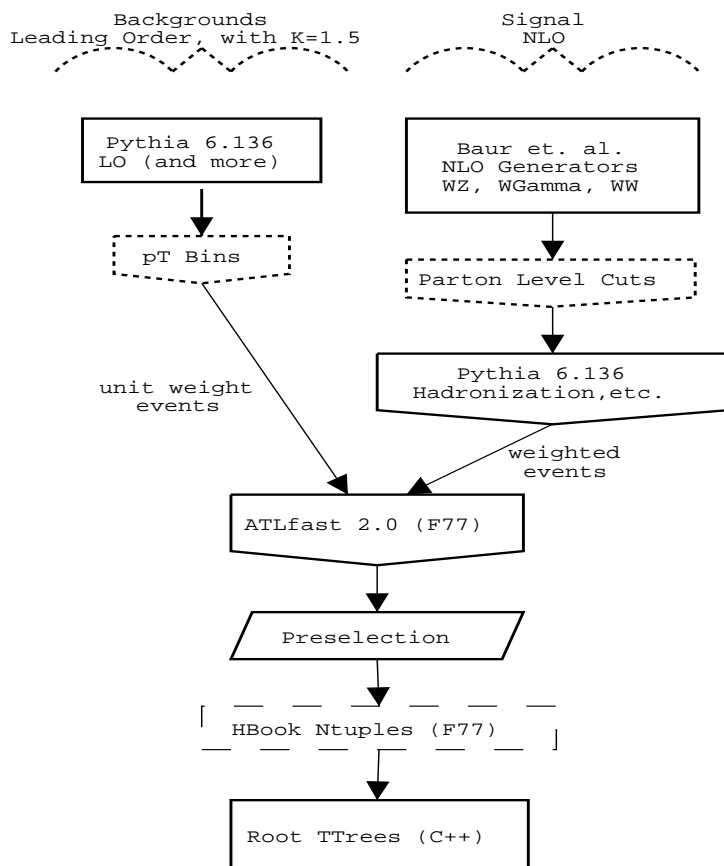


FIG. 3: The event generation chain is shown schematically for the background processes (left branch) and the signals (right branch).

For the purposes of this analysis, it will be useful to know the event weights as a function of the anomalous coupling parameters. The BHO generator has been modified to provide this information for each event, as discussed in the appendix of this paper.

The event simulation chain for the signal processes is presented in the right-hand branch of Figure 3. The generation parameters are as follows: The CTEQ4M [29] parton density functions and two loop expression for α_S are used with $\Lambda^{4, \overline{\text{MS}}} = 0.298$ GeV. The Z^0 and W^\pm masses are $M_Z = 91.187$ GeV and $M_W = 80.396$ GeV, the electroweak mixing angle is $\sin^2 \theta_W = 0.23$, and the electroweak coupling is $\alpha_{\text{QED}}(M_Z) = 1/128$. The Cabbibo angle is $\cos \theta_{\text{Cabbibo}} = 0.975$, with no third generation mixing.

B. Background Simulation

PYTHIA 6.136 has been used to simulate the background processes for this analysis. For most processes PYTHIA uses leading order matrix elements and higher order corrections are approximated with the parton shower. Considering the relatively small impact the backgrounds have on the analysis and the fact that the most important background— W +jet production—is modelled in PYTHIA at first order (tree level) in QCD, background simulations using next-to-leading order matrix elements are not expected to change the results significantly. The use of leading order background simulations has been accounted for by using rather pessimistic assumptions for assessing the systematic errors due to the background rates, which will be presented in Sec. V C.

To account for the effect NLO corrections will have on the total background rate, a single

constant k -factor of 1.5 has been applied to all of the background process event rates.

To ensure an adequate sampling of the backgrounds, the generation of each background is divided into phase space regions based on the transverse momentum (called ‘ P^T bins’) of the hard subprocess, and then the events from each region are combined afterwards. This ensures good statistics in the tails of the distributions. Whenever possible, a sample of events corresponding to an integrated luminosity $\mathcal{L} = 1000 \text{ fb}^{-1}$ has been generated (this is not possible for the low transverse momentum regions of large cross section processes like $b\bar{b}$, single- W , and single- Z —but the low transverse momentum regions are not nearly as significant as the high transverse momentum ones). Each event is simulated with `PYTHIA`, then passed to the ATLAS fast detector simulation program `ATLfast` (discussed in the next section), before being tested against a set of preselection cuts. Each event is permuted through the various particle mis-identification possibilities (wherein jets are mis-identified as electrons or photons, which will be described in Section III D), and events which pass the preselection are written to disk. This provides a large sample of events which can be used to fine tune the final selection cuts.

Details specific to the generation of individual background processes will be discussed in Section IV. The event simulation chain for the backgrounds is presented in the left-hand branch of Figure 3.

C. Detector Simulation

In the final stage of the simulation chain, the response of the ATLAS detector to the final state particles is modelled using the ATLAS fast simulation program `ATLfast` [30] version 2.55.

`ATLfast` selects isolated photons and charged leptons, reconstructs jets, and estimates the missing transverse energy in the event. The detector geometry is modelled using a simple parameterisation of the coverage for precision physics and calorimetry, and details about the electromagnetic calorimeter barrel/endcap transition region and the granularity of the calorimeters is included. For electrons, muons, and photons, a parameterisation of the detector resolution is used, but no reconstruction efficiencies are applied. In this study, these efficiencies have been accounted for by applying the relevant factors to the cross sections. Jets are reconstructed in `ATLfast` using a cone algorithm with $\Delta R = \sqrt{\Delta\eta^2 + \Delta\phi^2} = 0.4$, where η is the pseudo-rapidity and ϕ is the azimuthal angle. The resolution parameterisation includes the effect of the magnetic field on jet reconstruction and the expected jet reconstruction efficiencies, as determined from full simulation.

A complete description of the `ATLfast` detector simulation can be found in Ref. [30], including the specific parameterisations and a detailed comparison between full and fast simulation. A comprehensive description of the detector sub-systems can be found in Ref. [31] and references therein.

Before the output from `ATLfast` is written to file, the events are first required to pass a preselection (discussed in Section IV D) which ensures they have the basic properties of the signal signature. Besides the reconstructed event information from `ATLfast`, two other things are incorporated into these files: the ‘Monte Carlo truth’, which is the event record before detector simulation is applied, and the event weights as a function of the anomalous TGC parameters.

Efficiencies and Rejection Factors
$R_{J-\gamma} = 3200$
$R_{J-e^\pm} = 10^5$
$\epsilon_\gamma = 83\%$
$\epsilon_{e^\pm} = 73\%$
$\epsilon_{\mu^\pm} = 95\%$

TABLE I: ATLAS detector efficiencies and rejection factors which have been assumed for this study. $R_{J-\gamma}$ and R_{J-e^\pm} are the rejection factors for jets faking photons and electrons, and ϵ_γ , ϵ_{e^\pm} , and ϵ_{μ^\pm} are the efficiencies for reconstructing photons, electrons and muons.

D. Particle Identification in ATLAS

The contributions for many of the backgrounds depend directly on the detector's ability to distinguish one type of particle from another. Since the cross sections for processes with QCD jets in the final state are often several orders of magnitude higher than the cross section for the processes of interest, the most important contribution will be from jets mis-identified as either electrons or photons. In this section the rejection factors and efficiencies for particle identification with the ATLAS detector are reviewed. A summary is presented in Table I.

In ATLAS, photon identification will be based on the shower shape in the electromagnetic (EM) calorimeter, leakage into the hadron calorimeter, and a veto on charged tracks which line up with the EM deposition. Based on these criteria, the expected rejection factor for jets mis-identified as photons in the ATLAS detector has been studied in Ref. [31, Sec. 7.6] and [32]. The rejection factors, based on an efficiency of 83.0% (83.1%) for low (high) luminosity, increase with increasing E^T up to about 50 GeV, at which point the rejection plateaus. Based on these studies, a jet rejection $R_{J-\gamma} = 3200$ has been assumed for the present analysis, with a photon efficiency of $\epsilon_\gamma = 83\%$ (i.e. 1 out of 3200 jets will be mis-identified as a photon, and 83% of the true photons will be correctly identified). Since the completion of the present analysis, improvements in the jet rejection factors achievable by including isolation conditions (wherein the photon candidate is required to be isolated from other hadronic activity) have been demonstrated in Ref. [33]. The rejection factors are found to improve by about 50% to well over 4000 at high E^T without compromising the photon efficiency. As such, the rejection factor of 3200 which has been assumed here should be considered a conservative estimate.

Electron candidates will be selected in the ATLAS experiment using information from the calorimetry and inner detector. The expected rejection factor for jets mis-identified as electrons in the ATLAS detector has been studied in Ref. [31, Sec. 7.4] and [34]. By cutting on the ratio of energy deposition in the first and subsequent depths of the calorimetry, rejection based on shower length can be achieved. The very fine granularity in pseudo-rapidity of the ATLAS EM Accordion calorimeter can be used to identify substructures in the lateral shower profile. The EM cluster is then required to have a good inner detector track pointing to it. The energy measured by the calorimetry is required to match the momentum measured with the tracker. Cuts on the impact parameter are particularly useful for reducing contamination from photon conversions, which usually produce tracks which do not line up with the interaction point. Finally, loose transition radiation cuts are imposed. At low (high) luminosity a rejection factor of 150 000 (45 000) can be achieved for $P^T = 30$ GeV electrons with a reconstruction efficiency of 72.7% (67.5%). In the present study, a rejection factor $R_{J-e^\pm} = 10^5$ has been assumed with efficiency $\epsilon_{e^\pm} = 73\%$. The slightly smaller R_{J-e^\pm} is chosen to account for possible performance degradation which may occur at higher $P_{e^\pm}^T$, because the inner detector momentum resolution decreases with increasing P^T .

The efficiency for reconstructing muons using information from the muon spectrometer com-

binned with the inner detector peaks at about 97% at $P_{\mu^\pm}^T = 10$ GeV, and decreases slowly to about 85% at 1 TeV [31, Sec. 8.1.2.1]. This decrease in efficiency is due to the increase in probability (with increasing muon energy) for the muon to initiate electromagnetic showers. These localised showers can result in large numbers of hits in the muon system, which spoil the pattern recognition of the hit from the genuine muon. A constant muon efficiency $\epsilon_{\mu^\pm} = 95\%$ has been assumed for the present study. The rate of fake high P^T muons will be negligible in ATLAS [35].

The ATLAS fast simulation software **ATLfast** does not account for particle mis-identification in the reconstruction of Monte Carlo events. To simulate this effect, events are first reconstructed with the normal **ATLfast** algorithms, and then tested against the kinematic cuts. If the event passes the cuts, it is accepted with weight one. Subsequently, a copy of the event is created with one of the reconstructed jets re-labelled as a photon, and the event-copy is tested against the kinematic cuts. If the event-copy passes the kinematic cuts, the copy is accepted with weight $1/R_{J-\gamma}$. This procedure is repeated for each of the jets in the event. The same procedure is followed for the mis-identification of jets as electrons, but this time the event weight would be $1/R_{J-e^\pm}$.

IV. BACKGROUNDS AND EVENT SELECTION

The $WW\gamma$ vertex will be probed at ATLAS using the muon and electron decay channels of diboson production, $pp \rightarrow W^\pm\gamma \rightarrow l^\pm\nu\gamma$ where l^\pm denotes an electron or muon type lepton and ν is a neutrino or antineutrino. Hadronic decay channels are difficult to separate from QCD backgrounds, and the addition of these channels are not expected to significantly improve the precision of the measurements.

The signature in the detector is a high transverse momentum (P^T) charged lepton, high P^T photon, and large missing transverse momentum P_{miss}^T arising from the neutrino. There are several other processes which look similar in the detector (irreducible backgrounds), and others which look similar because some part of the event has been reconstructed incorrectly.

The trigger for $W\gamma$ events will be the single photon trigger, operating without pre-scaling at $P_\gamma^T = 40$ GeV and 60 GeV for low and high luminosity running respectively [31, Table 11-20]. This study is optimised for low luminosity. The precise setting for the trigger is not important, because the events of interest are in the kinematic region with $P_\gamma^T > 100$ GeV. As such, the results of this study do not depend strongly on the threshold of the P_γ^T trigger used for ATLAS.

The cross section for $W\gamma$ production diverges for small values of P_γ^T , which is the result of infrared singularities arising in photon emission from the incoming massless quarks. The Feynman diagram containing the TGC vertex (Figure 1, right) does not involve photon radiation from fermion lines, and thus very little sensitivity to the anomalous TGC's is lost by imposing a P^T cut on the photon transverse momentum.

In this section, we summarise the processes which contribute to the backgrounds and then present the kinematic cuts which optimise the selection of event candidates.

A. Backgrounds with a Lepton and Photon Signature

$W(\rightarrow \tau\nu)\gamma$ with leptonic tau decays The cross section for $W\gamma$ production with the W decaying to $\tau\nu_\tau$ is a factor two smaller than the signal. This irreducible process is essentially the same as the signal, and does contain the TGC vertex. However, since τ 's are more

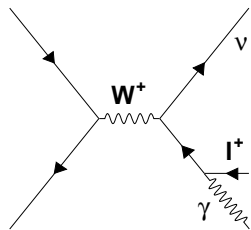


FIG. 4: The Feynman graph for radiative W decays is shown.

difficult to reconstruct, it is treated as a background in this study. The $\tau^\pm \rightarrow l^\pm \nu \bar{\nu}$ decay (for $l^\pm = \mu^\pm, e^\pm$) branching ratio is about 34%. The contribution from this process will be reduced by lepton transverse momentum cuts, because the secondary charged leptons from the τ -decay will have reduced transverse momentum as compared to the direct lepton from the W -decay. At Tevatron energy, this effect renders the leptonic τ decay background negligible [36]. Previous studies [37] have assumed that this also holds at LHC energy, and it will be shown here that this is not the case.

The process is simulated using the PYTHIA [28] 6.136 $W\gamma$ process (`MSUB(80)` switch in PYTHIA) and forcing the W decay to τ, ν . As for all of the backgrounds, the event generation uses leading order approximations for the cross sections and so a constant k -factor of 1.5 is applied to account for this.

Radiative W decays, $W^\pm \rightarrow l^\pm \nu \gamma$ This irreducible process, shown in Figure 4, should be included in an ideal Monte Carlo simulation of the signal. It interferes with the signal process wave functions, and is of the same order as the Born level process. However, this diagram is not included in any of the matrix elements available for $W\gamma$ production at NLO in QCD. The effect of omitting the diagram is small, so long as a kinematic cut is included which keeps the events far away from the kinematic region where this diagram becomes important. The contribution from the diagram is largest in the region where the lepton and photon are nearly collinear, and so a requirement on the separation of the lepton from the photon $\Delta R(l^\pm, \gamma) = \sqrt{\Delta\phi^2 + \Delta\eta^2}$ is effective for this purpose.

The process is simulated using PYTHIA 6.136 single- W production (`MSUB(1)` switch in PYTHIA) by forcing the W to decay to either $e\nu_e$ or $\mu\nu_\mu$ and allowing the photon to come from a final state shower of the charged lepton. There is no double counting with the $W\gamma$ process, because in that case the photon arises from the initial state quarks or from a TGC vertex. In generating this process initial state QCD radiation is turned off to avoid double counting with the W +jet process, which will be considered later. Generation of events in the kinematic region of interest has been sped up by enhancing the final state QED shower by a factor 20 (`PARJ(83)` parameter in PYTHIA), and ending the QED shower at a rather large invariant mass of 10 GeV (`PARJ(84)` parameter in PYTHIA). The event rate after kinematic cuts has been compared with a simulation which uses PHOTOS⁶ [38] 2.02, and good agreement is found.

$Z^0\gamma$ production with leptonic decays This diboson process looks similar to the signal when one of the two charged leptons escapes detection, either because it is outside of the central

⁶ PHOTOS estimates the size of QED bremsstrahlung in the leading-logarithmic approximation. It can be used in conjunction with any Monte Carlo generator for any type of decay.

region of the detector, has insufficient transverse momentum, or is simply missed because of lepton reconstruction efficiencies.

The process is simulated with the PYTHIA 6.136 $Z^0\gamma$ process (MSUB(19) switch in PYTHIA) by forcing the Z^0 to decay to charged leptons.

Heavy flavors $t\bar{t}(\gamma)$ and $b\bar{b}(\gamma)$ These heavy flavor processes typically have several jets in the final state. Nevertheless, since their cross sections are so large in comparison to the signal, a small fraction of the events having signal-like signatures can result in significant backgrounds. The lepton can be produced from leptonic bottom-meson decays or from $t \rightarrow Wb$ with the W decaying leptonically. These processes also contribute to the fake-lepton and fake-photon backgrounds, in the case where a jet is mis-identified as an electron or photon. The primary means of reducing the contributions from these processes is to cut on the jet activity in the events.

The heavy flavor processes are simulated with PYTHIA 6.136 (MSEL=5,6 switches in PYTHIA). The final states with and without a photon are generated separately. The $t\bar{t}\gamma$ and $b\bar{b}\gamma$ final states are simulated with the final state radiation enhanced in the same manner that was used for radiative W decays. For this sample, no jet-photon mis-identification is applied, as the real-photon is of interest here. The number of events passing the cuts has been checked against a simulation using PHOTOS for final state bremsstrahlung. A separate sample of events is generated using the $t\bar{t}$ and $b\bar{b}$ processes with QED showering turned off (so as to avoid double counting the phase space which has already been populated with the $t\bar{t}\gamma$ and $b\bar{b}\gamma$ final states), to account for the jet-photon mis-identification scenario. The contribution arising from mis-identified jets is significantly larger than the real photon contribution.

B. Jets Mis-identified as Electrons

Direct photon production, γ +jet This process mimics the signal in the case where the jet is mis-identified as an electron. Because there is no direct source of missing energy for this background, a cut on P_{miss}^T will be effective in reducing its contribution.

This process is simulated using the PYTHIA 6.136 processes $q\bar{q} \rightarrow \gamma g$, $g\bar{q}^{(-)} \rightarrow \gamma\bar{q}^{(-)}$, and $gg \rightarrow \gamma g$ (MSUB(14), MSUB(29), MSUB(115) switches in PYTHIA).

C. Jets Mis-identified as Photons

W +jet production The cross section for single- W production is over 10^4 times larger than that of the signal. When the final state jet fakes a photon, the signature for this process will be identical to that of the signal. This will be the most challenging background to $W\gamma$ production.

PYTHIA 6.136 processes $q\bar{q}' \rightarrow W^\pm g$ and $g\bar{q}^{(-)} \rightarrow W^\pm\bar{q}^{(-)}$ (MSUB(16), MSUB(31) switches in PYTHIA) with the W^\pm forced to decay to leptons are used to simulate this background.

Z^0 +jet production Because the cross section for this process is so large, the rare cases when the jet is mis-identified as a photon and the Z^0 decays leptonically with one charged lepton escaping detection, will be important.

PYTHIA 6.136 is used to simulate the process in the same manner as for W +jet production (`MSUB(15),MSUB(30)` switches in PYTHIA).

D. Event Selection and Efficiency

The simulation of the $W\gamma$ signal process is performed at NLO. The backgrounds are simulated at leading order, with higher order corrections entering through the parton shower. When performing the event selection, extra care must be taken to ensure none of the event selection criteria operate on the differences between the NLO and LO simulations. One example would be a cut on the number of jets reconstructed in the event. The NLO simulation does not use a parton shower—and so there is at most one coloured parton (coming from the order α_S emission) in the event. This parton is independently fragmented and hadronised using PYTHIA, and so it may be divided further into multiple jets, but the probability of this is considerably smaller than would be the case if the parton shower were used, and multiple coloured partons were present in the event before hadronization. This means that a cut on the number of jets reconstructed in the event (which would be a logical cut to use against the $t\bar{t}$ and $b\bar{b}$ backgrounds) is *not allowed*, because the signal simulation does not give a reasonable prediction of the number of jets in the event.

To ensure these differences in the simulation do not play a role in the choice of cuts, the kinematic cuts which are employed to maximise the signal purity are optimised using a leading order simulation of both the signal and backgrounds.

A preselection is applied to the events at generation time, and ensures the events have the basic properties of the signal signature. The $W\gamma$ analysis preselection requires exactly one high P^T isolated photon and exactly one high P^T isolated e^\pm or μ^\pm in the region of precision physics ($|\eta| < 2.5$). It further requires that the P_{miss}^T reconstruction is consistent with the hypothesis that the missing transverse momentum arises from a neutrino, which together with the charged lepton, reconstructs to the W -mass (this will be discussed in more detail in the appendix), i.e.

$W\gamma$ Preselection

$$\begin{aligned} &\text{one isolated photon, } P_\gamma^T > 80 \text{ GeV, } |\eta_\gamma| < 2.5 \\ &\text{one isolated electron or muon, } P_{l^\pm}^T > 20 \text{ GeV, } |\eta_{l^\pm}| < 2.5 \\ &\text{solution to neutrino longitudinal momentum exists.} \end{aligned} \tag{11}$$

The number of events remaining for $\mathcal{L} = 30 \text{ fb}^{-1}$ after the preselection are shown in the first column of Table II. The signal and background rates are similar after the selection. The numbers reported in this table employ the full NLO simulation for the signal, and a k -factor of 1.5 has been applied to the backgrounds, which are generated at leading order.

The goal of the present analysis is not to observe the signal process over the backgrounds (as would be the case for a search), but rather to obtain the maximum sensitivity to non-standard TGC couplings in the signal process. As such, the purpose of the kinematic cuts is not just to optimise the signal purity, but to optimise the contribution to the signal from the regions of phase space where anomalous TGC's affect the signal most. With this in mind, the sensitivity to the anomalous TGC's is also tabulated in Table II after each subsequent cut is applied. The sensitivity reported in this table is statistical only and a lower number represents a better sensitivity. The method for evaluating this sensitivity is not important for the present discussion, it will be presented in Sec. V B.

The first three kinematic cuts are imposed on the transverse momentum of the photon, lepton, and missing energy. These cuts do not improve nor degrade the sensitivity to the

	$W \rightarrow W\gamma \rightarrow$							
	$Z\gamma$	$W+\text{jet}$	$Z+\text{jet}$	$t\bar{t}(\gamma)$	$b\bar{b}(\gamma)$	$\gamma+\text{jet}$	$l\nu\gamma$	$\tau\nu\gamma$
preselection	2436	4367	7398	1561	253	956	20	710
$P_\gamma^T > 100$ GeV	1277	2097	2101	945	160	894	14	665
$P_{l^\pm}^T > 25$ GeV	1196	1938	1800	837	64	664	13	586
$P_{\text{miss}}^T > 25$ GeV	377	1557	215	689	43	44	12	574
$\Delta R(\gamma, l^\pm) > 1$	376	1543	183	611	42	44	12	574
$\sum_{\text{jets}} P_{\text{jet } j}^T < 100$ GeV	341	1280	133	286	26	11	12	534

	# events			Spread in Stat. 95% C.L.	
	Backgrounds	$W\gamma$ Signal	$\frac{S}{B}$	λ_γ	$\Delta\kappa_\gamma$
preselection	17701	17717	1.0	0.0076	0.18
$P_\gamma^T > 100$ GeV	8153	10638	1.30	0.0076	0.18
$P_{l^\pm}^T > 25$ GeV	7098	10066	1.42	0.0075	0.18
$P_{\text{miss}}^T > 25$ GeV	3511	7311	2.08	0.0074	0.18
$\Delta R(\gamma, l^\pm) > 1$	3385	6791	2.01	0.0074	0.18
$\sum_{\text{jets}} P_{\text{jet } j}^T < 100$ GeV	2623	4262	1.62	0.0066	0.15

TABLE II: The number of events surviving after each of the kinematic cuts is applied cumulatively for the $W\gamma$ analysis. An integrated luminosity $\mathcal{L} = 30 \text{ fb}^{-1}$ at the LHC has been assumed, and reconstruction efficiencies have been applied. The statistical spread in the 95% confidence intervals have been derived using a binned maximum likelihood fit to the P_γ^T distribution and the results are averaged over 1000 simulated ATLAS experiments.

anomalous TGC's because they are not isolating nor removing information which is relevant for the couplings (at small transverse momentum the effects of the anomalous TGC's on the matrix elements are extremely small). These cuts are designed to improve the signal purity. The smaller the background contribution is in the final sample, the less the results will depend upon our ability to properly model these backgrounds. The transverse momentum cuts are optimised by maximising the signal to background ratio using leading order simulations for both the signal and backgrounds, while monitoring the statistical sensitivity to the anomalous TGC's (using NLO simulations for the signal) to ensure the cut is not increased to a point where the sensitivity is degraded. As an example of when this can happen, consider the P_γ^T cut. If this cut were increased to values of the order 500 GeV, the signal to background (S/B) ratio would be very large, but information which is relevant for the anomalous TGC's (and in particular for the $\Delta\kappa_\gamma$ parameter) would be lost, and so the sensitivity would start to degrade. The transverse momentum cuts chosen for the photon, charged lepton, and missing energy are:

$$\begin{aligned}
P_\gamma^T &> 100 \text{ GeV}, \quad |\eta_\gamma| < 2.5 \\
P_{l^\pm}^T &> 25 \text{ GeV}, \quad |\eta_{l^\pm}| < 2.5 \\
P_{\text{miss}}^T &> 25 \text{ GeV}.
\end{aligned}
\tag{12}$$

The absence of additional high- P^T photons or charged leptons has already been ensured by the preselection. The exact location of these additional photon and charged lepton cuts has very little effect on the purity. Hard photons (or hard jets mis-identified as photons) are rare for the background processes, so the P_γ^T cut is effective at improving S/B by 30%. The P_{miss}^T cut greatly reduces the contributions from backgrounds ($Z+\text{jet}$ and $Z\gamma$) which do not produce direct neutrinos.

$\sum_{jets} P_{jet_i}^T$ [GeV]	S/B	S/ \sqrt{B}	Spread in 95% C.L.	
			λ_γ	$\Delta\kappa_\gamma$
no cut	2.0	120	0.00738	0.179
< 400	2.0	120	0.00653	0.158
< 300	2.0	110	0.00659	0.156
< 200	1.8	100	0.00644	0.151
< 150	1.8	96	0.00652	0.150
<u>< 100</u>	<u>1.6</u>	<u>83</u>	<u>0.00656</u>	<u>0.149</u>
< 75	1.6	77	0.00656	0.150
< 50	1.6	70	0.00670	0.150
< 40	1.6	66	0.00683	0.152
< 30	1.6	62	0.00696	0.155
< 20	1.8	57	0.00745	0.159
< 10	2.0	47	0.00773	0.168

TABLE III: The effect of the $\sum_{jets} P_{jet_i}^T$ cut on the sensitivity to anomalous TGC's, purity, and significance is tabulated for $W\gamma$ production. An integrated luminosity of 30 fb^{-1} is assumed and efficiencies have been applied. The statistical spread in the 95% confidence intervals have been derived using a binned maximum likelihood fit to the P_γ^T distribution and the results are averaged over 1000 simulated ATLAS experiments. The numbers reported in this table employ the full NLO simulation for the signal, and a k -factor of 1.5 has been applied to the backgrounds, which are generated at leading order.

As discussed in the previous section, the simulation of the signal has omitted the Feynman diagram arising from radiative W -decays. A cut on $\Delta R(\gamma, l^\pm)$ is included to ensure the signal events are far from the region of phase space where this diagram becomes non-negligible. Thus the motivation for this cut is purely to ensure this approximation, which has been made in the modelling of the signal, does not affect the final results. Note that the event rate coming from the radiative W -decay background is rather small from the onset. This is because isolation criteria has been applied in the reconstruction phase, and so is already part of the preselection.

The last cut which is applied operates on the jet activity in the event and is included to optimise the sensitivity to the anomalous TGC's. NLO corrections degrade the sensitivity to the TGC couplings because a large number of extra diagrams are included in the calculation, the majority of which do not include the TGC vertex. The NLO corrections become largest when the jet activity is large. This means that a cut on P_{jet}^T will serve to moderate the influence of these extra diagrams. When P_{jet}^T is small, the signal is Born-like. When it is large, the diboson system will be recoiling against a hard central jet, and the influence of the TGC vertex will be minimal.

Because the signal is generated at NLO and the backgrounds are generated at LO, care must be taken when applying a cut such as this. The distribution of P_{jet}^T at NLO for diboson production is most accurately interpreted as the inclusive jet transverse momentum. This means that the cut should not operate on a particular jet (e.g. the hardest or second hardest jet), but rather on the vector sum of the jet activity, $\sum_{jets} \vec{P}_{jet_i}^T$. It should be stressed that this is necessary because of the fixed order approach which has been used to model the signal, and would not be true if a calculation accurate to all orders were possible.

The $\sum_{jets} P_{jet_i}^T$ cut is optimised strictly on the basis of the sensitivity to the anomalous TGC's. The sensitivity as a function of the cut is shown in Table III. As the cut is increased, the purity goes down, but at the same time the sensitivity increases. This is because the signal itself (in kinematic regions where the anomalous TGC's have little effect) is washing out the sensitivity. At about 100 GeV, the sensitivity begins to be degraded by the cut. This is the value which is chosen.

After all kinematic cuts have been applied, the signal exceeds the backgrounds by a factor 1.6. About 6900 event candidate will be observed with an integrated luminosity of 30 fb^{-1} , 2600 of these events will be background. The dominant background is W +jet production, with

<u>$W\gamma$ Selection</u>
one isolated photon, $P_\gamma^T > 100$ GeV, $ \eta_\gamma < 2.5$
no other photon with $P_\gamma^T > 80$ GeV, $ \eta_\gamma < 2.5$
one isolated electron or muon, $P_{l^\pm}^T > 25$ GeV, $ \eta_{l^\pm} < 2.5$
no other charged lepton with $P_{l^\pm}^T > 20$ GeV, $ \eta_{l^\pm} < 2.5$
$P_{\text{miss}}^T > 25$ GeV
$\sum_{\text{jets}} P_{\text{jet } i}^T < 100$ GeV
$\Delta R(l^\pm, \gamma) = \sqrt{\Delta\phi^2 + \Delta\eta^2} > 1$
solution to neutrino longitudinal momentum exists

TABLE IV: The kinematic cuts imposed for the $W\gamma$ analysis are presented.

the jet mis-identified as a photon. Further improvements in the separation of jets from photons (as have already been achieved in Ref. [33]) will help to reduce this background. The diboson processes $Z\gamma$ and $W(\tau^\pm, \nu)\gamma$ are significant backgrounds as well, with $W(\tau, \nu)\gamma$ being the second most important background. It is unlikely that its contribution can be further reduced by other cuts. Since the $W(\tau^\pm, \nu)\gamma$ channel is sensitive to the TGC vertex and contributes a non-negligible amount to the $l^\pm, \gamma, P_{\text{miss}}^T$ final state, future analyses at the LHC may benefit by accounting for the effects anomalous TGC couplings would have on this process, by treating it as a signal rather than a background.

The final selection cuts for the $W\gamma$ analysis are summarised in Table IV.

V. ANALYSIS METHODS AND RESULTS

Having established the procedure for obtaining a sample of diboson event candidates, the goal is to establish the degree to which the data is consistent with the Standard Model prediction for the three gauge-boson couplings. This comparison of the data to theory is quantified by means of the λ and $\Delta\kappa$ parameters of the most general gauge-invariant CP conserving Lagrangian for the TGC interaction (Eq. 1).

In anticipation of the ATLAS experiment data, there are two scenarios to prepare for: the anomalous TGC parameters could be in agreement with the Standard Model values within experimental errors, or non-standard couplings might be observed. In the former scenario, limits may be placed on the anomalous TGC parameters. In the latter, the collaboration will be in a position to measure the characteristics of the couplings, i.e. disentangle the contributions from the different anomalous TGC parameters and study their energy dependence.

This section focuses on how to perform measurements of the three gauge-boson couplings and the radiation zero with ATLAS experiment data. Many of the methods which will be discussed in this section will require the reconstruction of event kinematics, including the four momentum of the final state neutrino from the W -decay. This reconstruction is discussed in the appendix.

A. Observing the Radiation Zero at LHC

The radiation zero has been discussed in Section II B, where it was suggested that the ‘signed’ rapidity separation (see Eq. 5) of the photon from the charged lepton arising in the W^\pm decay would be the best distribution for observing this electroweak effect at the LHC. In this section

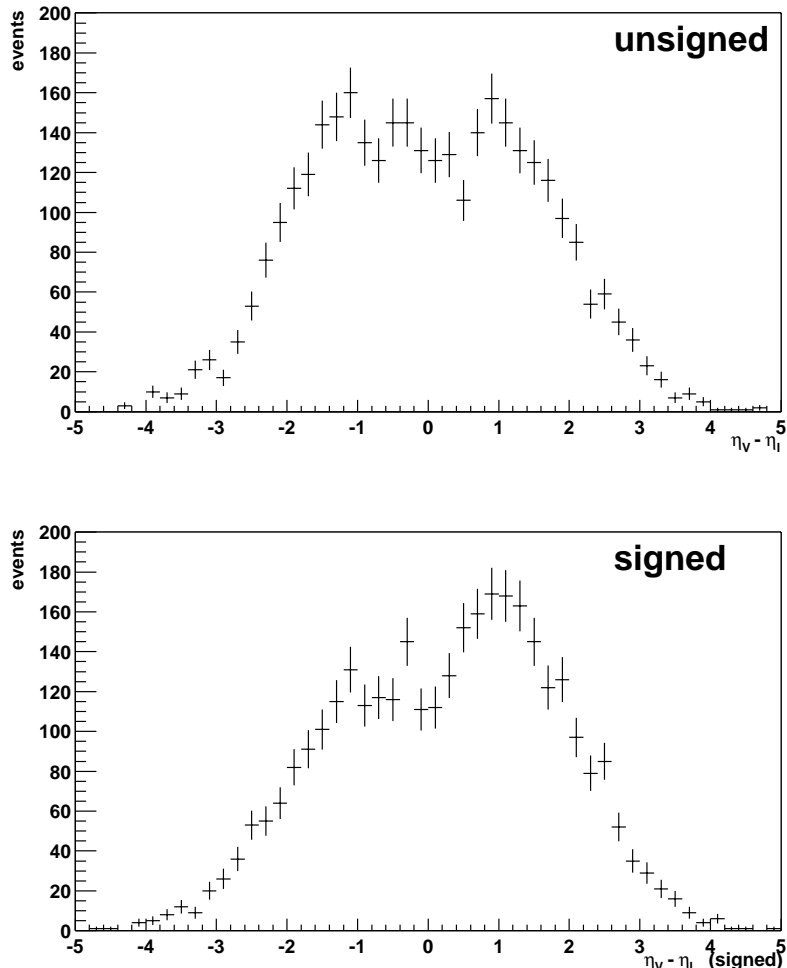


FIG. 5: The rapidity separation (top) of the photon from the charged lepton is shown for $W\gamma$ production at the LHC. For the bottom distribution the rapidity separation has been ‘signed’ according to Eq. 5. The kinematic cuts of Sec. IV have been applied, with the exception of the jet veto, for which the transverse momentum is changed to $\sum_{jets} P_{jet_i}^T < 30$ GeV. The points with error bars represent “mock” data for one ATLAS experiment with integrated luminosity of 30 fb^{-1} . This data has been simulated using the SM TGC parameters, and includes the background contributions.

the relevant distributions are presented for 30 fb^{-1} of LHC data, so as to evaluate the prospects for observing this Standard Model signature with ATLAS.

The kinematic cuts for this part of the analysis are identical to those of the TGC analysis, with one exception. The transverse momentum for the jet veto is made more stringent, $\sum_{jets} P_{jet_i}^T < 30$ GeV, as compared to the $\sum_{jets} P_{jet_i}^T < 100$ GeV veto which is used for the TGC analysis. This change is imposed because the radiation zero is a leading order effect, and so hard central jets tend to ‘fill in’ the radiation zero, masking its signature. The stringent jet veto effectively recovers the leading order behaviour.

In Figure 5 the signed and unsigned $W\gamma$ production rapidity separation distributions are shown for an integrated luminosity of 30 fb^{-1} from one simulated ATLAS experiment. This data has been simulated using SM TGC parameters, and includes the background contribu-

tions. The radiation zero is already evident in the unsigned distribution. In addition, for the signed distribution, the characteristic radiation zero asymmetry is also visible. Using 30 fb^{-1} of integrated luminosity, the radiation zero will be observable at LHC.

B. Methods for Measuring Anomalous Coupling Parameters

In this section we outline the methods which can be used to extract anomalous TGC confidence intervals.

The simplest method for looking for non-standard effects in the $WW\gamma$ coupling is the “counting method”. The diboson production matrix elements depend linearly on the anomalous TGC parameters, which results in a quadratic dependence for the event rate. By comparing the observed number of events to the expected event rate, the degree of compatibility with the Standard Model can be ascertained and limits can be set on the anomalous TGC parameters. This is one of the methods which has been used by the UA2 collaboration in Ref. [39]. The sensitivity for this method at hadron colliders is washed out by the low P_γ^T region, where the cross section is large, and the effects of anomalous TGC’s are small. For this reason, a considerable advantage can be obtained by introducing kinematic cuts restricting the measurement to the high P_γ^T region. This has been studied at leading order for $W\gamma$ and WZ production at ATLAS in Ref. [5], where it has been shown that statistical limits comparable (within about a factor 1.5) to what will be presented in this paper can be obtained. The primary disadvantage of the counting method technique is that the results depend directly on the overall normalisation, and thus are very sensitive to systematic uncertainties such as the luminosity measurement, the theoretical knowledge of higher order QCD corrections, and the internal proton structure. The uncertainty in the luminosity may be as high as 10% at LHC, NNLO corrections have yet to be calculated and are expected to be large at high transverse momentum due to the opening of the gg channel, and our knowledge of the structure functions is at about the 2-5% level. For these reasons, competitive limits on the anomalous TGC’s using this technique would be very difficult, and would certainly require a significant improvement in theoretical modelling of the diboson processes. Systematic effects such as these were not taken into account for the limits reported in Ref. [5]. A further disadvantage of the technique is that if non-standard results are observed, it gives very little information as to where the source of the deviation comes from, and thus would make disentangling the contributions from the various anomalous TGC’s difficult. This method is not the most promising avenue for establishing confidence limits on the anomalous TGC’s, and is not explored further here.

Measurements of the anomalous couplings can be made by using the maximum likelihood method to compare the experimentally observed spectrum of a kinematic observable (such as the transverse momentum of the photon, P_γ^T) to Monte Carlo reference distributions which are known as a function of the anomalous TGC parameters (the technique for constructing the reference histograms is presented in the appendix). Since each of the events that is produced by the signal simulation for this study has a (positive or negative) weight associated with it, an unbinned maximum likelihood fit is not possible, and we are forced to use the binned method.

For simplicity, we choose to arbitrarily reduce the number of anomalous TGC parameters by setting some of the parameters to their Standard Model values. When only one (two) anomalous TGC parameter(s) is left free in the estimation, this is referred to as a one (two) parameter estimate.

As an example of a maximum likelihood fit to a one dimensional distribution, the transverse momentum distribution of the photon in $W\gamma$ production is shown in Figure 6, after applying

the kinematic cuts described in Section IV. The points with error bars represent “mock” data for one ATLAS experiment with integrated luminosity of 30 fb^{-1} . This data has been simulated using the SM TGC parameters, and includes the background contributions. The “mock” data histogram is constructed by sampling each bin according to a Poisson distribution with the mean given by the relevant bin content of the SM reference histogram. The lines in Figure 6 (bottom) are the reference distributions (i.e. theoretical expectation) for several choices of the anomalous TGC parameters. The contribution of backgrounds to the reference distributions is shown as a shaded histogram, and does not depend on the anomalous TGC parameters. The one and two parameter negative log likelihood curves are shown as a function of the λ_γ and $\Delta\kappa_\gamma$ parameters with the 68, 90, and 95% confidence limits indicated. These confidence limits correspond to the single experiment which has been simulated for this figure. When another ATLAS experiment is simulated, the confidence limits will be different, on account of statistical fluctuations (indeed it is the sensitivity of the distribution to these fluctuations which the likelihood method measures). If many such experiments are simulated, only 68% of the simulated experiments will yield results which are consistent with the input parameters (SM couplings in this case) to within one standard deviation. In order to obtain the best estimate of the limits that will be achieved at ATLAS, it is necessary to average the confidence limits over many simulated ATLAS experiments (the limits tabulated in this paper are averaged over 5000 simulated experiments). The fluctuation in these confidence limits represents the confidence with which the confidence limits are known (or the *error on the error*), and is not studied here.

The P_γ^T distribution is very sensitive to the anomalous TGC’s because it projects out central production angles and large diboson invariant masses. In Figure 7 the transverse mass distribution (refer to Eq. A.24) for $W\gamma$ production is shown, which is a directly observable quantity that is sensitive mostly to the energy dependence of the anomalous couplings. A distribution which is sensitive to the gauge-boson helicity states is the transverse momentum of the lepton in $W\gamma$ production, which is shown in Figure 8.

Rather than using a projection of the event kinematic configurations onto a single distribution to estimate the anomalous TGC parameters, one can extract more information about the data by using the maximum likelihood method with multi-dimensional histograms.

The limiting factor in extrapolating to higher dimensional fits is the computer time required to generate the reference distributions. If each histogram dimension has N bins, and there are d dimensions, then the computational time scales as N^d . The computer time⁷ necessary to generate adequate statistics for one dimensional histograms is the order of a day (this includes generating millions of events using the NLO matrix elements, hadronising the events—which consumes most of the computer time, and fast simulation in the detector). Since each histogram dimension might typically be divided into 50 bins, the amount of computer time necessary in moving from 1 to 2 dimensional histograms becomes cumbersome, and the computer time for 3 dimensions is unreasonable (≥ 1 year).

In order to produce reference histograms for two dimensional distributions in a reasonable amount of time, the number of bins in each dimension is reduced. Thus increasing the number of dimensions in the fit is a trade-off: sensitivity is gained because of the information contained in the extra dimension, and sensitivity is lost because of the reduced granularity in the binning of each dimension.

An example of parameter estimation using a two-dimensional maximum likelihood fit is shown in Figure 9, where the angular and energy degrees of freedom are projected out separately

⁷ The computer times quoted here are for a 650 MHz Pentium III processor.

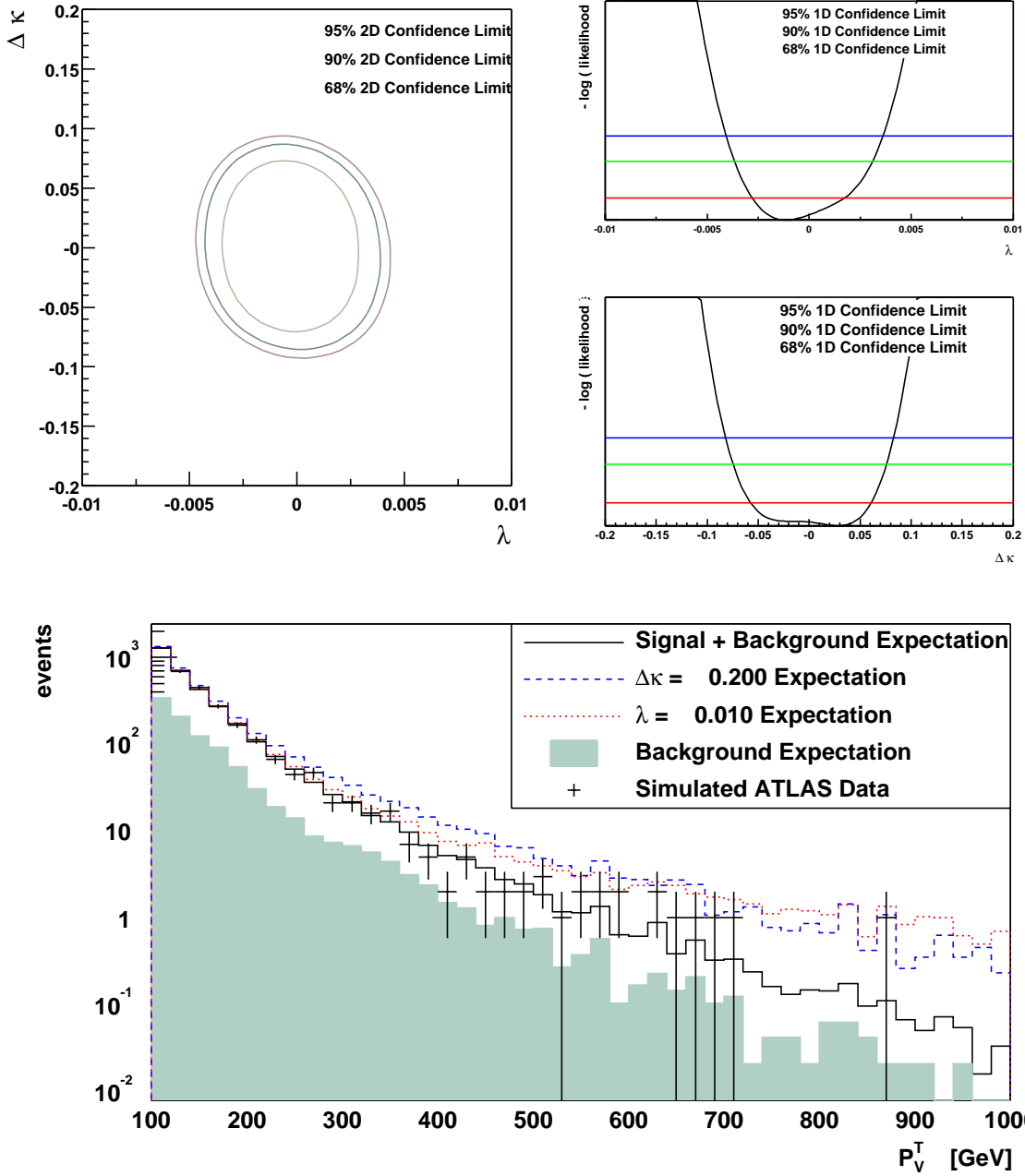


FIG. 6: The transverse momentum distribution of the photon in $W\gamma$ production is shown (bottom), after applying the kinematic cuts described in Section IV. The points with error bars represent “mock” data for one ATLAS experiment with integrated luminosity of 30 fb^{-1} . This data has been simulated using the SM TGC parameters, and includes the background contributions. The lines are the reference distributions for several choices of the anomalous TGC parameters. The contribution of backgrounds to the reference distributions is shown as a shaded histogram, and does not depend on the anomalous TGC parameters. The one (top right) and two (top left) parameter negative log likelihood curves are shown as a function of the λ_γ and $\Delta\kappa_\gamma$ parameters with the 68, 90, and 95% confidence limits indicated. These confidence limits correspond to the single experiment which has been simulated for this figure.

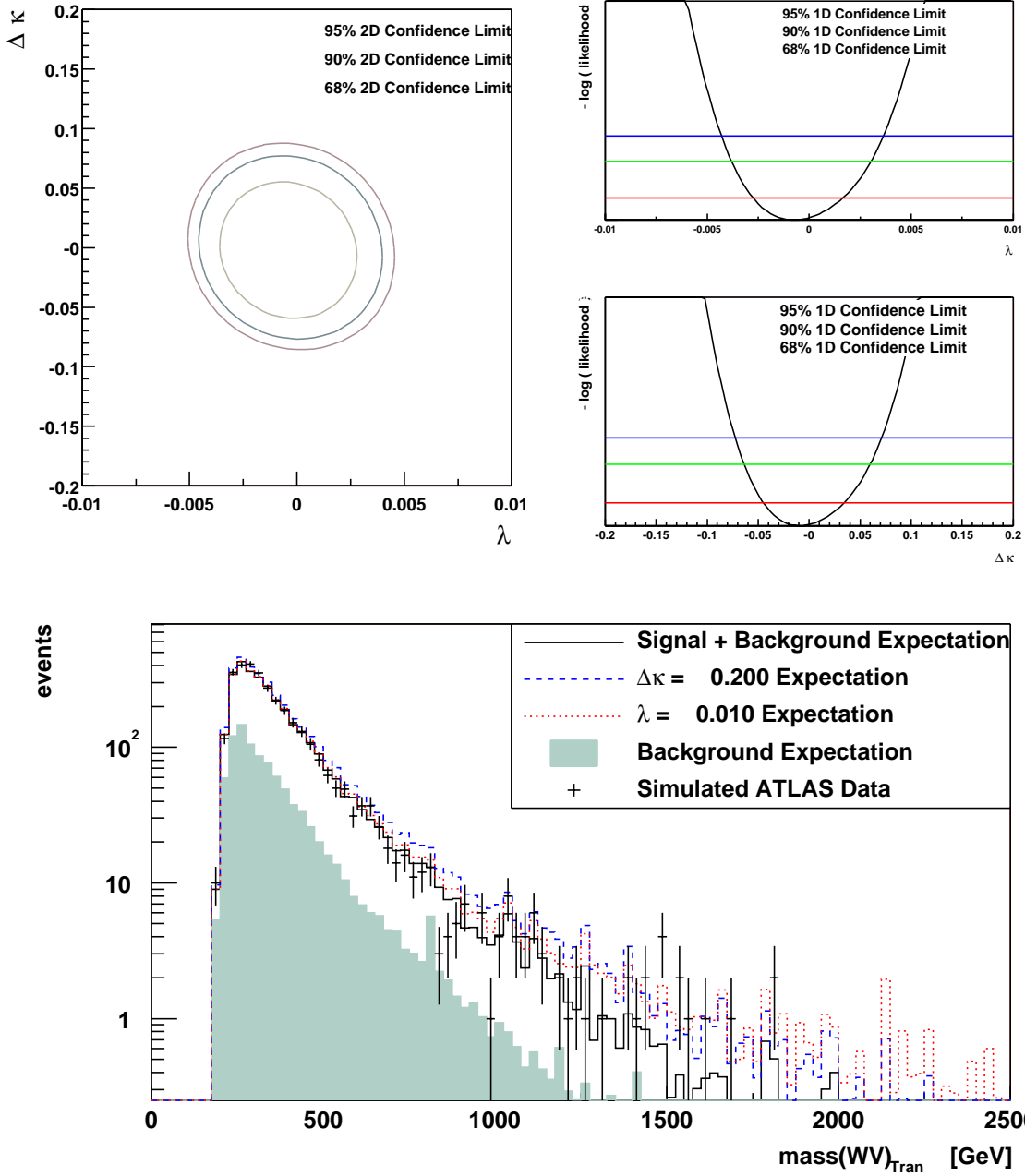


FIG. 7: The transverse mass distribution in $W\gamma$ production is shown (bottom), after applying the kinematic cuts described in Section IV. The points with error bars represent “mock” data for one ATLAS experiment with integrated luminosity of 30 fb^{-1} . This data has been simulated using the SM TGC parameters, and includes the background contributions. The lines are the reference distributions for several choices of the anomalous TGC parameters. The contribution of backgrounds to the reference distributions is shown as a shaded histogram, and does not depend on the anomalous TGC parameters. The one (top right) and two (top left) parameter negative log likelihood curves are shown as a function of the λ_γ and $\Delta\kappa_\gamma$ parameters with the 68, 90, and 95% confidence limits indicated. These confidence limits correspond to the single experiment which has been simulated for this figure.

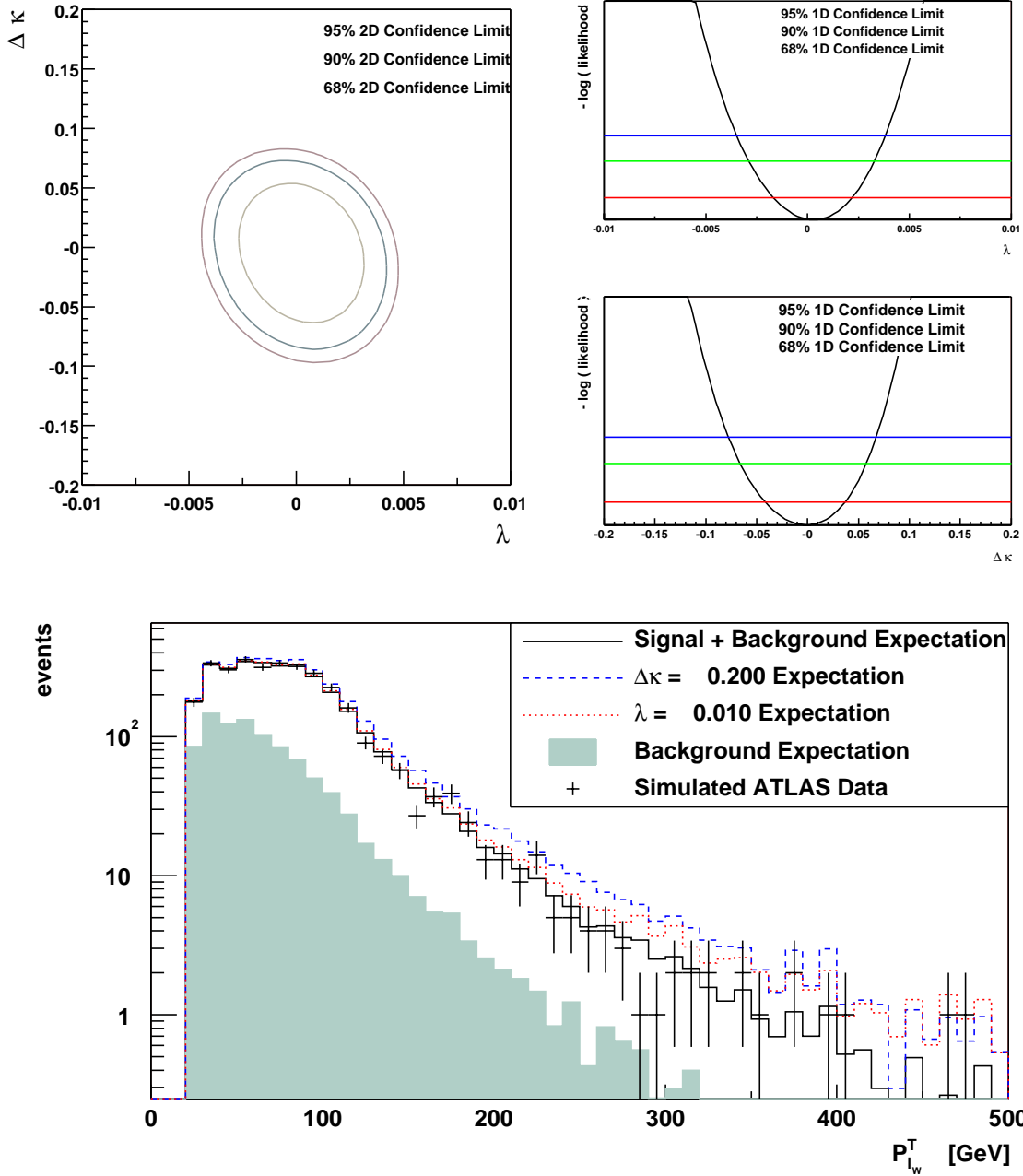


FIG. 8: The transverse momentum distribution of the charged lepton in $W\gamma$ production is shown (bottom), after applying the kinematic cuts described in Section IV. The points with error bars represent “mock” data for one ATLAS experiment with integrated luminosity of 30 fb^{-1} . This data has been simulated using the SM TGC parameters, and includes the background contributions. The lines are the reference distributions for several choices of the anomalous TGC parameters. The contribution of backgrounds to the reference distributions is shown as a shaded histogram, and does not depend on the anomalous TGC parameters. The one (top right) and two (top left) parameter negative log likelihood curves are shown as a function of the λ_γ and $\Delta\kappa_\gamma$ parameters with the 68, 90, and 95% confidence limits indicated. These confidence limits correspond to the single experiment which has been simulated for this figure.

in a 2 dimensional histogram of the diboson invariant mass (reconstructed using both solutions, as in Eq. A.23) versus the reconstructed centre-of-mass frame photon production angle (as for the invariant mass, the centre-of-mass reconstruction has two solutions, and both solutions are included in the histogram).

The confidence limits derived from the distributions will be presented in Section VD. Before a meaningful comparison of the various distribution's sensitivity to anomalous TGC's can be made, the systematic contributions must be evaluated, which is the subject of the next section.

C. Systematic Uncertainties

The LHC will provide an unprecedented event rate for diboson production. It is important to understand to what extent a measurement of anomalous TGC parameters is limited by statistics (i.e. limited by the size of the data sample) and to what extent it is limited by systematics, such as our understanding of the detector, or our ability to model the theory which is being tested. In this section, the contributions of the various systematic effects to the confidence limits are evaluated.

As described in Sec. VB, the expected statistical confidence limits are extracted by comparing histograms which represent 'mock' ATLAS data to reference histograms which are evaluated as a function of the anomalous TGC parameters. For the evaluation of each systematic contribution, the histograms which represent the 'mock' ATLAS data have been replaced with histograms which use a different model assumption. The reference histogram assumptions *are not changed*. Thus, for example, to evaluate the systematic effect a change in the background rate has on the confidence limits, the background process cross sections are increased (or decreased) in the data histograms, but are left unchanged in the reference histograms. The change in the model assumptions causes a shift in the preferred value for each anomalous TGC parameter. This shift is independent of luminosity and is taken as an estimate of the systematic error.

This is a worst case scenario strategy for evaluating the systematic effects because it assumes that a mis-modelling of some effect (the background rate in this example) has occurred, and that it has not been possible to correct for this mis-modelling. A more likely scenario for the ATLAS measurement of the TGC couplings is that significant mis-modelling does exist (for example in the cross-section for the W +jet background process), but these model-assumptions will be independently extracted from the data, such that the modelling can be corrected.

Before describing the various contributions to the systematic errors, a few comments are in order concerning the manner in which the model assumptions are changed. Several of the systematics can be evaluated in the manner described above without re-generating the reference histograms from which the "mock" data is sampled with Poisson statistics. An example is the systematic arising from the modelling of the backgrounds, which is evaluated by simply changing the normalisation of the background contributions in the reference histograms. Other systematics are evaluated by re-generating the reference histograms, and so the systematic shift in the preferred anomalous TGC parameters receives contributions from the systematic effect being studied, but also from statistical fluctuations in the reference histograms. This second contribution results in an uncertainty on the knowledge of the systematic effect $\Delta\sigma_{\text{syst}}$ (an "error on the error"). For each anomalous TGC, $\Delta\sigma_{\text{syst}}$ is evaluated by replacing the 'mock' ATLAS data histograms with histograms which use a *the same* model assumption, but are derived from a different sample of Monte Carlo events. In cases where the systematic effects are a significant fraction of the total confidence interval, $\Delta\sigma_{\text{syst}}$ is small.

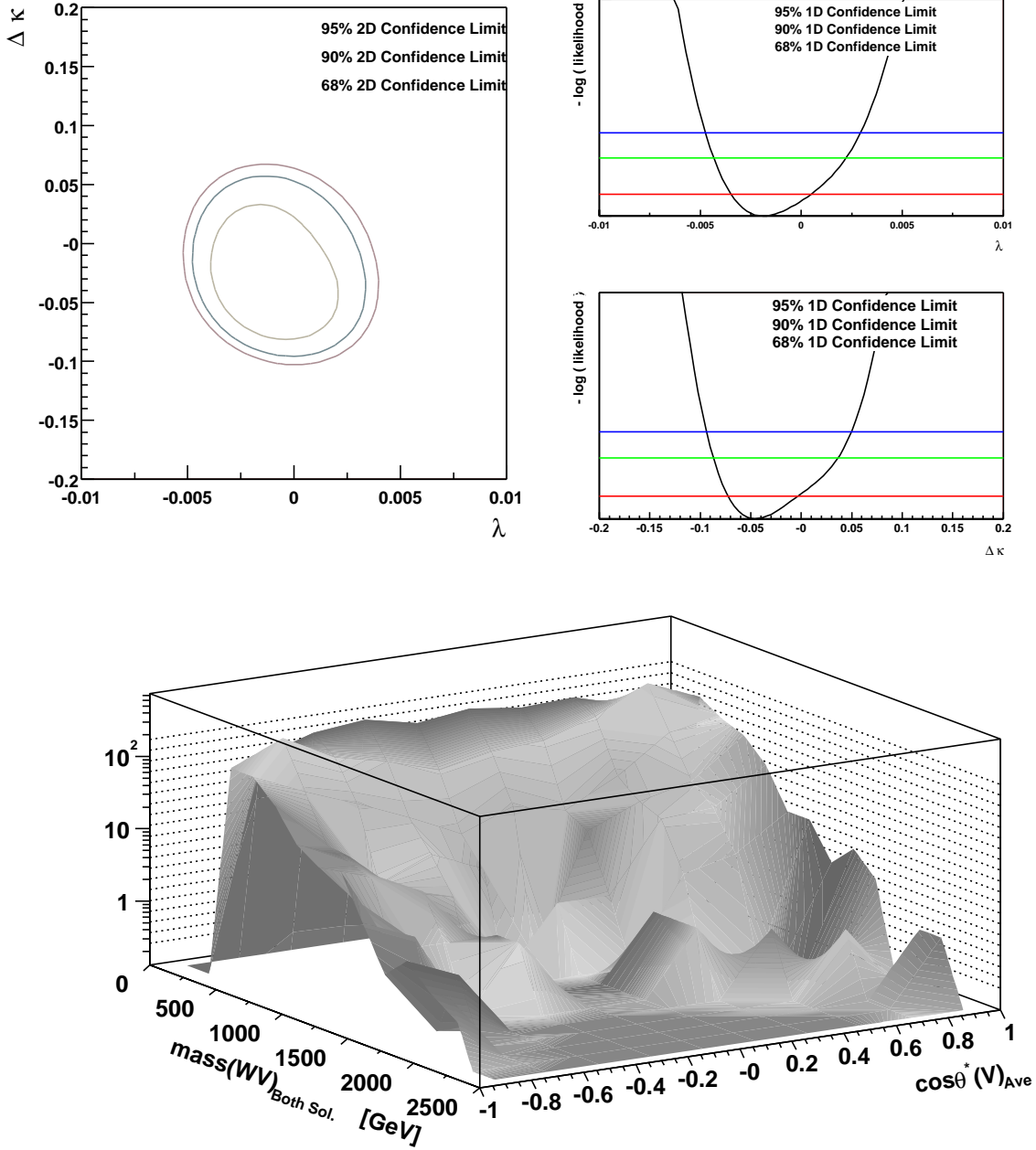


FIG. 9: The reconstructed diboson invariant mass (both solutions, Eq. A.23) versus the reconstructed centre-of-mass frame photon production angle (both solutions are included in the histogram) for $W\gamma$ production is shown (bottom), after applying the kinematic cuts described in Section IV for the Standard Model reference histogram (including contributions from backgrounds) assuming an integrated luminosity of 30 fb^{-1} . The one (top right) and two (top left) parameter negative log likelihood curves are shown as a function of the λ_γ and $\Delta\kappa_\gamma$ parameters with the 68, 90, and 95% confidence limits indicated. These confidence limits correspond to the single experiment which has been simulated for this figure. The amount of computer time necessary to produce this distribution rises exponentially with the number of dimensions, which necessitates the use of a coarse binning granularity.

In the following sections, the systematics will be evaluated using a binned maximum likelihood fit to the P_γ^T distribution (see Fig. 6). The 95% statistical confidence intervals derived from this distribution are $-0.0033 < \lambda_\gamma < 0.0033$ and $-0.073 < \Delta\kappa_\gamma < 0.076$. Tables enumerating the systematic effects for other distributions will be presented afterwards.

Background rate systematics

NLO calculations have been used for the computer modelling of the signal process to account for the significant modifications higher order corrections have on the distributions in the physical region of interest for TGC studies. However, only leading order event generators have been used for the backgrounds (new Monte Carlo tools are now becoming available which will make NLO simulations more accessible for studies like this one, such as the new generator for $p\bar{p}^{(-)} \rightarrow Z + X \rightarrow l^+l^- + X$ which has been developed by one of the authors in Ref. [40]).

To partially account for this discrepancy, a single constant k -factor of 1.5 has been applied to all backgrounds. This is slightly larger than the k -factor expected for hadronic single gauge-boson production (1.4), and is probably a reasonable ‘average’ guess for the k -factors of the background processes which are significant for diboson production.

The systematic effect of the background rate has been evaluated by varying this background process k -factor in the ‘mock’ data histograms from 1.5 up to 2 and down to 1. The statistical 95% confidence interval for the λ_γ parameter in $W\gamma$ production is $-0.0033 < \lambda_\gamma < 0.0033$, and a change of the background k -factor in the ‘mock’ data histograms to 1 (2) produces a -0.00025 (0.00011) shift on the mean value of λ_γ preferred by the ‘mock’ data. This shift is the same order of magnitude as $\Delta\sigma_{\text{sys}} = \pm 0.00025$, and provides a negligible contribution to the total confidence interval. For the case of the $\Delta\kappa_\gamma$ parameter, a change of the background k -factor in the ‘mock’ data histograms to 1 (2) produces a 0.0043 (-0.014) shift on the mean value of $\Delta\kappa_\gamma$ preferred by the ‘mock’ data. Though this will make background modelling the single largest contribution to the $\Delta\kappa_\gamma$ systematic errors, it is nevertheless small compared to the statistical confidence intervals for $\Delta\kappa_\gamma$, which are a factor five or more larger.

Parton density function systematics

The CTEQ4 [29] parton density functions⁸ (p.d.f.’s) have been used for the reference and ‘mock’ data histograms in this study. To evaluate the systematic effects associated with the mis-modelling of p.d.f.’s, the CTEQ4 p.d.f.’s have been replaced with the CTEQ3 [41] series p.d.f.’s in the ‘mock’ data histograms.

The phenomenological p.d.f.’s are estimated from experimental data, by fitting the p.d.f.’s to the data constrained by the theoretical expectation for the Bjorken momentum fraction x and scale Q evolution. The change in the phenomenological structure functions from one series to the next for a specific p.d.f. author group (e.g. the difference between CTEQ3 and CTEQ4) reflects the change that an increase in the available experimental data has on the p.d.f.’s. This change is an indication of the mis-modelling which existed in the older p.d.f. set which was of importance to the newly collected data. As such, this difference is

⁸ Newer versions of the p.d.f.’s, including CTEQ5 and CTEQ6 are now available.

taken as a reasonable estimate for how the p.d.f.'s might evolve over the course of LHC running.⁹

The systematic shift on the mean value of the λ_γ ($\Delta\kappa_\gamma$) parameter preferred by the ‘mock’ data due to changing the p.d.f. from CTEQ4 to CTEQ3 is 0.00042 (0.0029) which is about 13% (4%) as large as the 95% statistical confidence limit of $-0.0033 < \lambda_\gamma < 0.0033$ ($-0.073 < \Delta\kappa_\gamma < 0.076$). The p.d.f.'s provide a small contribution to the total confidence interval for either parameter.

Systematics arising from neglected higher orders

The effect of neglecting higher order diagrams (for our signal this would be order $\alpha_S^{\geq 2}$ diagrams) is traditionally evaluated by varying the (somewhat arbitrarily chosen) renormalisation and factorisation scales up and down by a factor 2. This is also the strategy which has been adopted here.

The systematic shift on the mean value of the λ_γ parameter preferred by the ‘mock’ data due to multiplying the factorisation and renormalisation scales by a factor $\frac{1}{2}$ (2) is 0.00107 (0.00093). This provides the dominant systematic effect for the λ_γ parameter measurement. For the $\Delta\kappa_\gamma$ parameter, the shift of 0.00022 (0.00063) is small in comparison to other systematic effects.

Detector effects

The modelling of the ATLAS detector will affect the measurements and confidence intervals for anomalous couplings. For example, if the reconstructed transverse momentum of photons was systematically shifted upward, then it would appear as if an excess of events was observed at high P_γ^T , which is the characteristic signature of anomalous TGC's.

The systematic effects associated with detector modelling are evaluated for this study in a very simple manner. The analysis has been repeated assuming a fictional ‘perfect’ detector. A fictional detector such as this is easily simulated by simply turning off the detector smearing in the event generation software chain. The mean shift of the TGC parameters preferred by the ‘mock’ data (simulated with the fictional ‘perfect’ detector) is then evaluated by comparing them to reference histograms which use the standard ATLAS fast detector simulation.

The effect is largest for the $\Delta\kappa_\gamma$ TGC parameter. This parameter is enhanced by an amount proportional only to the diboson mass (c.f. Eqs. 2-3), and so it receives a more even contribution from the full spectrum of events, as compared to the λ_γ parameter, which derives its sensitivity primarily from just the highest P^T events.

For the case of the λ_γ and $\Delta\kappa_\gamma$ parameters the shift is -0.00018 and 0.0055 respectively. This shift is small compared to the statistical 95% confidence limits of $-0.0033 < \lambda_\gamma < 0.0033$ and $-0.073 < \Delta\kappa_\gamma < 0.076$.

Note that this evaluation of the detector systematics takes into account the reconstruction of the events, but not detector effects which would affect the event rates. Since the

⁹ The LHC machine will explore regions of Bjorken x and scale q which have never before been probed experimentally. This means a considerable change in the p.d.f.'s is likely to occur in these newly explored regions when the LHC data becomes available. This large change in the p.d.f.'s will be of little concern for a study such as this one, because the change will be corrected for in the reference histograms. For the present study, the concern is with mis-modelling of the p.d.f.'s after this initial change has occurred.

analysis does not use information from the overall normalisation, a change in the total event rate will not affect the measurements (hence the luminosity need not be considered). However, a change which effects the background rates differently from the signal rates would produce an effect on the measurements. One example of a detector effect like this would be the rejection rate of jets faking photons or electrons in the detector. This, however, has already been taken into account with the systematic effects in the background rate.

D. Results and Comparison of Methods

Having derived the statistical confidence limits and enumerated the systematic effects, it is now possible to assess the various methods for extracting measurements of the anomalous TGC parameters.

The systematic effects described in the previous sections are uncorrelated, and so the individual shifts¹⁰ are added together in quadrature to obtain the total systematic error for the measurements. An enumeration of the systematic effects is presented in Tables V and VI. The total systematic error is then added in quadrature to the statistical 95% confidence intervals to obtain the confidence intervals which define the ATLAS experiment sensitivity to the anomalous TGC parameters. These intervals are presented in Tables VII and VIII, assuming an integrated luminosity of 30 fb⁻¹. The definition of the various distributions are summarised in Table IX.

In Ref. [7], a variation on the method of Optimal Observables [42] is derived and applied to anomalous TGC measurements in the WZ channel. For completeness, we include the sensitivity of Optimal Observables for the $W\gamma$ channel in Tables V-VIII. Maximum likelihood fits to the Optimal Observable distribution are not competitive for the $WW\gamma$ anomalous TGC parameters. The Optimal Observable requires reconstruction of the full event, which significantly increases the effects of detector related systematics. Optimal Observable are not discussed further here, the interested reader is referred to the discussion in Ref. [7].

A maximum likelihood fit to the photon transverse momentum distribution P_γ^T has been the conventional means of extracting limits on the anomalous coupling parameters at hadron colliders (e.g. SPS, Tevatron). For both the λ_γ and $\Delta\kappa_\gamma$ parameters, the P_γ^T distribution provides the best limits. The reason for this is twofold: (1) The P_γ^T observable is sensitive to both angular and energy information, mimicking the behaviour which the λ_γ parameter affects on the matrix elements (Eq. 3). (2) The P_γ^T observable has the further advantage of being reconstructible without any assumptions or ambiguities which would otherwise be necessary to determine the centre-of-mass system.

For the λ_γ , the P_γ^T distribution provides the best limits even when systematic effects are neglected, whereas slightly better statistical precision can be achieved for the $\Delta\kappa_\gamma$ parameter

¹⁰ Some of the systematic effects (such as the change in the renormalisation and factorisation scale for λ_γ) produce a shift which goes only in one direction (i.e. a variation of the scale up or down by a factor 2, shifts the λ_γ parameter in the positive direction for both cases). This is because the likelihood function is often-times nearly symmetric about $\lambda_\gamma=0$. In cases such as these (or when only a single shift is reported such as for the p.d.f. systematic), the systematic effect is assumed to go in both directions (the systematic errors which have been used in the combination with statistical limits are reported in parentheses in the tables which follow). For example, the systematic shift produced by varying the scale by a factor $\frac{1}{2}$ and 2 for the λ_γ parameter extracted from the P_γ^T distribution is 0.00107 and 0.00093. The systematic error which has been assumed in this case is $[\pm\max(|0.00107|, |0.00093|)] = (-0.00107, 0.00107)$.

		Background $k = 2, k = 1$	PDF	Scale $\times 2, \times \frac{1}{2}$	Detector	\oplus All Systematics
P_γ^T	λ	0.00011,-0.00025 (-0.00025,0.00011)	0.00042 (-0.00042,0.00042)	0.00093,0.00107 (-0.00107,0.00107)	-0.00018 (-0.00018,0.00018)	(-0.00119,0.00117) $\Delta\sigma_{\text{syst}} = \pm 0.00025$
P_γ^T	$\Delta\kappa$	-0.0136,0.00425 (-0.0136,0.00425)	0.00288 (-0.00288,0.00288)	0.00063,0.00022 (-0.00063,0.00063)	0.00552 (-0.00552,0.00552)	(-0.015,0.00756) $\Delta\sigma_{\text{syst}} = \pm 0.00509$
P_{1W}^T	λ	-0.00042,0.00252 (-0.00042,0.00252)	0.002 (-0.002,0.002)	0.00133,0.00092 (-0.00133,0.00133)	0.00279 (-0.00279,0.00279)	(-0.00371,0.00446) $\Delta\sigma_{\text{syst}} = \pm 0.000941$
P_{1W}^T	$\Delta\kappa$	0.00089,-0.1 (-0.1,0.00089)	0.0704 (-0.0704,0.0704)	0.0275,0.0463 (-0.0463,0.0463)	0.115 (-0.115,0.115)	(-0.174,0.142) $\Delta\sigma_{\text{syst}} = \pm 0.0196$
P_{miss}^T	λ	0.00232,-0.00026 (-0.00026,0.00232)	-0.00121 (-0.00121,0.00121)	0.00052,0.00121 (-0.00121,0.00121)	0.00016 (-0.00016,0.00016)	(-0.00174,0.00289) $\Delta\sigma_{\text{syst}} = \pm 0.000307$
P_{miss}^T	$\Delta\kappa$	-0.0708,0.0267 (-0.0708,0.0267)	0.0234 (-0.0234,0.0234)	-0.00031,-0.0129 (-0.0129,0.0129)	0.0332 (-0.0332,0.0332)	(-0.0826,0.0503) $\Delta\sigma_{\text{syst}} = \pm 0.00743$
mass($W\gamma$) _{Both Sol.}	λ	-0.00058,0.00015 (-0.00058,0.00015)	0.00382 (-0.00382,0.00382)	0.00319,-0.00214 (-0.00214,0.00319)	0.00091 (-0.00091,0.00091)	(-0.00451,0.00506) $\Delta\sigma_{\text{syst}} = \pm 0.00201$
mass($W\gamma$) _{Both Sol.}	$\Delta\kappa$	0.00925,-0.00853 (-0.00853,0.00925)	-0.0202 (-0.0202,0.0202)	-0.0427,0.0656 (-0.0427,0.0656)	0.0431 (-0.0431,0.0431)	(-0.0644,0.0816) $\Delta\sigma_{\text{syst}} = \pm 0.044$
mass($W\gamma$) _{Min}	λ	-9e-05,0.00144 (-9e-05,0.00144)	0.00397 (-0.00397,0.00397)	0.0035,0.00419 (-0.00419,0.00419)	0.00211 (-0.00211,0.00211)	(-0.00615,0.00631) $\Delta\sigma_{\text{syst}} = \pm 0.00221$
mass($W\gamma$) _{Min}	$\Delta\kappa$	0.0161,-0.0321 (-0.0321,0.0161)	-0.0485 (-0.0485,0.0485)	0.0897,0.0869 (-0.0897,0.0897)	-0.0192 (-0.0192,0.0192)	(-0.109,0.105) $\Delta\sigma_{\text{syst}} = \pm 0.0137$
mass($W\gamma$) _{Tran}	λ	-7e-05,0.00111 (-7e-05,0.00111)	0.00386 (-0.00386,0.00386)	0.00062,0.00484 (-0.00484,0.00484)	0.0013 (-0.0013,0.0013)	(-0.00633,0.00642) $\Delta\sigma_{\text{syst}} = \pm 0.000728$
mass($W\gamma$) _{Tran}	$\Delta\kappa$	0.0261,-0.044 (-0.044,0.0261)	-0.0607 (-0.0607,0.0607)	-0.0298,-0.0498 (-0.0498,0.0498)	-0.0235 (-0.0235,0.0235)	(-0.0931,0.0861) $\Delta\sigma_{\text{syst}} = \pm 0.0114$
$\eta_\gamma - \eta$	λ	0.00946,-0.00241 (-0.00241,0.00946)	0.00305 (-0.00305,0.00305)	-0.00071,0.0159 (-0.00071,0.0159)	0.0108 (-0.0108,0.0108)	(-0.0115,0.0216) $\Delta\sigma_{\text{syst}} = \pm 0.00528$
$\eta_\gamma - \eta$	$\Delta\kappa$	0.0532,-0.178 (-0.178,0.0532)	-0.0338 (-0.0338,0.0338)	-0.0176,0.095 (-0.0176,0.095)	0.0655 (-0.0655,0.0655)	(-0.193,0.132) $\Delta\sigma_{\text{syst}} = \pm 0.0244$
$\cos\theta^*(\gamma)_{Ave}$	λ	0.00765,-0.0017 (-0.0017,0.00765)	-0.0045 (-0.0045,0.0045)	-0.00189,0.0138 (-0.00189,0.0138)	0.0103 (-0.0103,0.0103)	(-0.0115,0.0194) $\Delta\sigma_{\text{syst}} = \pm 0.00291$
$\cos\theta^*(\gamma)_{Ave}$	$\Delta\kappa$	0.0483,-0.131 (-0.131,0.0483)	-0.209 (-0.209,0.209)	-0.0273,0.0978 (-0.0273,0.0978)	0.0725 (-0.0725,0.0725)	(-0.258,0.246) $\Delta\sigma_{\text{syst}} = \pm 0.0193$
Opt Obs(λ) _{min mass}	λ	-0.00536,0.0028 (-0.00536,0.0028)	0.00416 (-0.00416,0.00416)	0.00039,0.00313 (-0.00313,0.00313)	0.00637 (-0.00637,0.00637)	(-0.00982,0.00869) $\Delta\sigma_{\text{syst}} = \pm 0.00139$
Opt Obs(κ) _{min mass}	$\Delta\kappa$	-0.0385,0.00173 (-0.0385,0.00173)	0.0596 (-0.0596,0.0596)	-0.0133,0.0469 (-0.0133,0.0469)	0.091 (-0.091,0.091)	(-0.116,0.118) $\Delta\sigma_{\text{syst}} = \pm 0.019$

TABLE V: The systematic errors for the $W\gamma$ production anomalous TGC parameters at the LHC are enumerated (continued in Table VI). The precision to which the systematic errors are known is denoted by $\Delta\sigma_{\text{syst}}$ in the last column.

		Background $k = 2, k = 1$	PDF	Scale $\times 2, \times \frac{1}{2}$	Detector	\oplus All Systematics
P_γ^T vs. P_{lW}^T	λ	-0.00022,0.00032 (-0.00022,0.00032)	0.00098 (-0.00098,0.00098)	-0.00099,0.00062 (-0.00099,0.00062)	0.00018 (-0.00018,0.00018)	(-0.00142,0.00122) $\Delta\sigma_{\text{sys}} = \pm 0.000392$
P_γ^T vs. P_{lW}^T	$\Delta\kappa$	-0.0107,0.0299 (-0.0107,0.0299)	0.0319 (-0.0319,0.0319)	0.0133,0.0078 (-0.0133,0.0133)	0.0223 (-0.0223,0.0223)	(-0.0425,0.0508) $\Delta\sigma_{\text{sys}} = \pm 0.00744$
mass($W\gamma$) _{Tran} vs. $ \eta_\gamma - \eta $	λ	0.00049,-0.00075 (-0.00075,0.00049)	0.00077 (-0.00077,0.00077)	0.00155,8e-05 (-0.00155,0.00155)	0.0007 (-0.0007,0.0007)	(-0.00201,0.00193) $\Delta\sigma_{\text{sys}} = \pm 0.000301$
mass($W\gamma$) _{Tran} vs. $ \eta_\gamma - \eta $	$\Delta\kappa$	0.0328,-0.0372 (-0.0372,0.0328)	0.00116 (-0.00116,0.00116)	0.0177,0.0548 (-0.0548,0.0548)	0.032 (-0.032,0.032)	(-0.0736,0.0715) $\Delta\sigma_{\text{sys}} = \pm 0.0176$
mass($W\gamma$) _{Min} vs. $ \eta_\gamma - \eta $	λ	0.00052,-0.00073 (-0.00073,0.00052)	0.0007 (-0.0007,0.0007)	0.00128,0.00299 (-0.00299,0.00299)	0.00066 (-0.00066,0.00066)	(-0.00322,0.00318) $\Delta\sigma_{\text{sys}} = \pm 0.000433$
mass($W\gamma$) _{Min} vs. $ \eta_\gamma - \eta $	$\Delta\kappa$	0.0335,-0.0364 (-0.0364,0.0335)	0.00874 (-0.00874,0.00874)	0.00746,0.0543 (-0.0543,0.0543)	0.0324 (-0.0324,0.0324)	(-0.0735,0.0721) $\Delta\sigma_{\text{sys}} = \pm 0.014$
mass($W\gamma$) _{Both Sol.} vs. $\cos\theta^*(\gamma)_{Ave}$	λ	0.00031,-0.00037 (-0.00037,0.00031)	0.00079 (-0.00079,0.00079)	0.00128,0.00128 (-0.00128,0.00128)	0.00047 (-0.00047,0.00047)	(-0.00162,0.00161) $\Delta\sigma_{\text{sys}} = \pm 0.000354$
mass($W\gamma$) _{Both Sol.} vs. $\cos\theta^*(\gamma)_{Ave}$	$\Delta\kappa$	0.0279,-0.0204 (-0.0204,0.0279)	0.00696 (-0.00696,0.00696)	-0.0082,0.0586 (-0.0082,0.0586)	0.0327 (-0.0327,0.0327)	(-0.04,0.073) $\Delta\sigma_{\text{sys}} = \pm 0.0133$

TABLE VI: Continuation of Table V.

by using multi-dimensional distributions.

Though the P_γ^T distribution encodes angular and energy information, helicity state information of the gauge-bosons is missing, which motivates the use of the 2-dimensional distribution P_γ^T vs. P_{lW}^T . This 2-dimension distribution uses a coarse binning granularity such that the bins are a factor 5 wider. It is this coarse granularity which keeps the 2-dimensional P_γ^T vs. P_{lW}^T distribution from showing an improvement over the single dimension P_γ^T distribution. The P_γ^T vs. P_{lW}^T distribution is also reconstructible without assumptions or ambiguities, and systematic effects are also small, indicating that slight improvements in the confidence limits may be possible using this distribution by focusing computer resources on improving the granularity of the 2 dimensional P_γ^T vs. P_{lW}^T reference histograms.

Detector related systematics for both parameters are small in comparison to the theoretical systematics. For an integrated luminosity of 30 fb^{-1} , the systematics are smaller than the statistical error by a factor 3 or more.

The expected 95% confidence intervals for the λ_γ and $\Delta\kappa_\gamma$ parameters using the P_γ^T distribution are

$$-0.0033_{\text{stat.}}, -0.0012_{\text{sys.}} < \lambda_\gamma < +0.0033_{\text{stat.}}, +0.0012_{\text{sys.}} \quad (13)$$

$$-0.073_{\text{stat.}}, -0.015_{\text{sys.}} < \Delta\kappa_\gamma < +0.076_{\text{stat.}}, +0.0076_{\text{sys.}} \quad (14)$$

which gives

$$-0.0035 < \lambda_\gamma < 0.0035 \quad (15)$$

$$-0.075 < \Delta\kappa_\gamma < 0.076 \quad (16)$$

when the statistical and systematic contributions are added in quadrature.

	95% Statistical Limit	\oplus All Systematics	95% Confidence Limit (stat \oplus syst)
P_γ^T	$-0.00328 < \lambda < 0.0033$ λ spread= 0.00657	(-0.00119,0.00117)	$-0.00349 < \lambda < 0.0035$ λ spread= 0.00698
P_γ^T	$-0.0732 < \Delta\kappa < 0.0761$ $\Delta\kappa$ spread= 0.149	(-0.015,0.00756)	$-0.0747 < \Delta\kappa < 0.0764$ $\Delta\kappa$ spread= 0.151
P_{lw}^T	$-0.00461 < \lambda < 0.00479$ λ spread= 0.0094	(-0.00371,0.00446)	$-0.00591 < \lambda < 0.00655$ λ spread= 0.0125
P_{lw}^T	$-0.0969 < \Delta\kappa < 0.0926$ $\Delta\kappa$ spread= 0.189	(-0.174,0.142)	$-0.199 < \Delta\kappa < 0.17$ $\Delta\kappa$ spread= 0.369
P_{miss}^T	$-0.00486 < \lambda < 0.00506$ λ spread= 0.00992	(-0.00174,0.00289)	$-0.00516 < \lambda < 0.00583$ λ spread= 0.011
P_{miss}^T	$-0.0786 < \Delta\kappa < 0.0955$ $\Delta\kappa$ spread= 0.174	(-0.0826,0.0503)	$-0.114 < \Delta\kappa < 0.108$ $\Delta\kappa$ spread= 0.222
mass($W\gamma$) _{Both Sol.}	$-0.00531 < \lambda < 0.00582$ λ spread= 0.0111	(-0.00451,0.00506)	$-0.00696 < \lambda < 0.00771$ λ spread= 0.0147
mass($W\gamma$) _{Both Sol.}	$-0.0744 < \Delta\kappa < 0.123$ $\Delta\kappa$ spread= 0.197	(-0.0644,0.0816)	$-0.0984 < \Delta\kappa < 0.148$ $\Delta\kappa$ spread= 0.246
mass($W\gamma$) _{Min}	$-0.00456 < \lambda < 0.00487$ λ spread= 0.00943	(-0.00615,0.00631)	$-0.00765 < \lambda < 0.00797$ λ spread= 0.0156
mass($W\gamma$) _{Min}	$-0.0712 < \Delta\kappa < 0.0972$ $\Delta\kappa$ spread= 0.168	(-0.109,0.105)	$-0.13 < \Delta\kappa < 0.143$ $\Delta\kappa$ spread= 0.273
mass($W\gamma$) _{Tran}	$-0.00425 < \lambda < 0.00435$ λ spread= 0.0086	(-0.00633,0.00642)	$-0.00762 < \lambda < 0.00776$ λ spread= 0.0154
mass($W\gamma$) _{Tran}	$-0.0698 < \Delta\kappa < 0.0914$ $\Delta\kappa$ spread= 0.161	(-0.0931,0.0861)	$-0.116 < \Delta\kappa < 0.126$ $\Delta\kappa$ spread= 0.242
$\eta_\gamma - \eta_l$	$-0.0179 < \lambda < 0.0137$ λ spread= 0.0316	(-0.0115,0.0216)	$-0.0212 < \lambda < 0.0256$ λ spread= 0.0468
$\eta_\gamma - \eta_l$	$-0.085 < \Delta\kappa < 0.0829$ $\Delta\kappa$ spread= 0.168	(-0.193,0.132)	$-0.211 < \Delta\kappa < 0.155$ $\Delta\kappa$ spread= 0.366
$\cos\theta^*(\gamma)_{Ave}$	$-0.016 < \lambda < 0.0131$ λ spread= 0.0292	(-0.0115,0.0194)	$-0.0198 < \lambda < 0.0234$ λ spread= 0.0432
$\cos\theta^*(\gamma)_{Ave}$	$-0.266 < \Delta\kappa < 0.0941$ $\Delta\kappa$ spread= 0.36	(-0.258,0.246)	$-0.371 < \Delta\kappa < 0.264$ $\Delta\kappa$ spread= 0.635
Opt Obs(λ) _{min mass}	$-0.00754 < \lambda < 0.00649$ λ spread= 0.014	(-0.00982,0.00869)	$-0.0124 < \lambda < 0.0108$ λ spread= 0.0232
Opt Obs(κ) _{min mass}	$-0.0876 < \Delta\kappa < 0.0783$ $\Delta\kappa$ spread= 0.166	(-0.116,0.118)	$-0.145 < \Delta\kappa < 0.142$ $\Delta\kappa$ spread= 0.287

TABLE VII: The 95% confidence intervals for $W\gamma$ production anomalous TGC parameters at the LHC assuming an integrated luminosity of 30 fb^{-1} (continued in Table VIII).

	95% Statistical Limit	\oplus All Systematics	95% Confidence Limit (stat \oplus syst)
P_γ^T vs. P_{lw}^T	$-0.00337 < \lambda < 0.00344$ λ spread= 0.00682	(-0.00142,0.00122)	$-0.00366 < \lambda < 0.00365$ λ spread= 0.00731
P_γ^T vs. P_{lw}^T	$-0.0685 < \Delta\kappa < 0.0722$ $\Delta\kappa$ spread= 0.141	(-0.0425,0.0508)	$-0.0806 < \Delta\kappa < 0.0883$ $\Delta\kappa$ spread= 0.169
mass($W\gamma$) _{Tran} vs. $ \eta_\gamma - \eta_l $	$-0.00346 < \lambda < 0.00346$ λ spread= 0.00692	(-0.00201,0.00193)	$-0.004 < \lambda < 0.00396$ λ spread= 0.00796
mass($W\gamma$) _{Tran} vs. $ \eta_\gamma - \eta_l $	$-0.0638 < \Delta\kappa < 0.0611$ $\Delta\kappa$ spread= 0.125	(-0.0736,0.0715)	$-0.0974 < \Delta\kappa < 0.094$ $\Delta\kappa$ spread= 0.191
mass($W\gamma$) _{Min} vs. $ \eta_\gamma - \eta_l $	$-0.00348 < \lambda < 0.00352$ λ spread= 0.007	(-0.00322,0.00318)	$-0.00474 < \lambda < 0.00475$ λ spread= 0.00949
mass($W\gamma$) _{Min} vs. $ \eta_\gamma - \eta_l $	$-0.0635 < \Delta\kappa < 0.0613$ $\Delta\kappa$ spread= 0.125	(-0.0735,0.0721)	$-0.0971 < \Delta\kappa < 0.0946$ $\Delta\kappa$ spread= 0.192
mass($W\gamma$) _{Both Sol.} vs. $\cos\theta^*(\gamma)_{Ave}$	$-0.00349 < \lambda < 0.00356$ λ spread= 0.00704	(-0.00162,0.00161)	$-0.00385 < \lambda < 0.0039$ λ spread= 0.00775
mass($W\gamma$) _{Both Sol.} vs. $\cos\theta^*(\gamma)_{Ave}$	$-0.065 < \Delta\kappa < 0.0627$ $\Delta\kappa$ spread= 0.128	(-0.04,0.073)	$-0.0763 < \Delta\kappa < 0.0962$ $\Delta\kappa$ spread= 0.173

TABLE VIII: Continuation of Table VII.

E. Controlling Systematics

The evaluation of systematic errors for this study has been performed using “worst case scenarios” in most instances. In this section a method for controlling the systematic effects which contribute to the confidence levels is explored.

By neglecting the normalisation when extracting the anomalous couplings, uncertainties due to luminosity are removed. An important systematic effect comes from our limited knowledge of QCD corrections, which dominates the systematics for λ_γ .

The issue is, if data is observed which differs from our reference histogram expectation, is it possible to determine whether the difference arises from anomalous couplings, or from something else such as mis-modelled QCD effects?

The calculation employed for the signal Monte Carlo is exact up to next-to-leading order QCD. It is expected that as a calculation is performed at successively higher orders, the calculation will become more precise (i.e. we assume the series converges). Further, it is expected that the effect of adding each new order is usually smaller than the effect of adding the previous order (e.g. the difference in going from NLO to NNLO will be smaller than the difference in going from LO to NLO). One conservative way¹¹ to estimate the error associated with neglected higher orders is to find the change in the result when going from the second-highest to the highest calculated order. In the present study, only two orders of QCD calculations exist: LO and NLO, so the differences between LO and NLO represent the uncertainty due to neglected orders.

¹¹ It is more common—and considered more appropriate—to vary the factorisation scale up and down by a factor of two (the factor 2 being convention only), which is the method that has been used to assign a quantitative number to systematic error associated with neglected higher orders in this study, see Sec. V C.

<u>1 dimension distributions</u>		# Bins
P_γ^T	transverse momentum of the photon	70
$P_{l_W}^T$	transverse momentum of the charged lepton from the W^\pm decay	50
P_{miss}^T	missing transverse momentum	50
$\text{mass}(W\gamma)_{Both\ Sol.}$	diboson invariant mass, each solution is histogrammed with weight $\frac{1}{2}$, (Eq. A.23)	100
$\text{mass}(W\gamma)_{Min}$	smaller of the two solutions for the diboson invariant mass (Eq. A.21)	100
$\text{mass}(W\gamma)_{Tran}$	$(l_W\gamma; P_{miss}^T)$ cluster transverse mass (Eq. A.24)	100
$\eta_\gamma - \eta_l$	pseudorapidity separation of the γ / Z^0 and the lepton from the W^\pm decay	50
$\cos\theta^*(\gamma)_{Ave}$	cosine of the production angle for the γ / Z^0 with respect to the beam-line in the reconstructed diboson center-of-mass frame, each of the two solutions are included with weight $\frac{1}{2}$	40
<u>Optimal Observables</u>		
$\text{Opt Obs}(\kappa)_{min\ mass}$	the OO (see Ref. [7]) using the $\Delta\kappa_\gamma$ parameter and the ν solution which gives the smaller diboson mass	100
$\text{Opt Obs}(\lambda)_{min\ mass}$	the OO (see Ref. [7]) using the λ_γ parameter and the ν solution which gives the smaller diboson mass	100
<u>2 dimension distributions</u>		
P_γ^T vs. $P_{l_W}^T$	transverse momentum of the photon vs. transverse momentum of the l_W	14×10
$\text{mass}(W\gamma)_{Tran}$ vs. $ \eta_\gamma - \eta_l $	diboson transverse mass vs. the pseudorapidity separation of the γ / Z^0 and l_W	15×10
$\text{mass}(W\gamma)_{Both\ Sol.}$ vs. $\cos\theta^*(\gamma)_{Ave}$	the diboson invariant mass vs. the production angle of the photon in the center-or-mass frame, each of the two solutions are included with weight $\frac{1}{2}$	15×10

TABLE IX: Definition of the distributions which are used to extract the confidence intervals for anomalous TGC's in Tables V-VIII. The number of bins used for the histograms of each distribution are shown on the right side of the table.

To illustrate this scenario, a set of reference histograms have been generated according to our usual model parameters using the BHO NLO generator. These histograms encompass our knowledge of the Standard Model, and the effects anomalous couplings have on that model. Rather than comparing this model to data generated using the same model, it is compared to data generated at LO (with Parton Shower) using the Pythia 6.136 Monte Carlo. The LO data has been normalised to the NLO expectation, such that only changes in distribution shapes are relevant. The usual kinematic cuts have been imposed, with the exception of the jet veto

which is removed so as to emphasise the difference in the simulations. The P_γ^T distribution and resulting confidence limits are shown in Figure 10, for an integrated luminosity of 100 fb^{-1} .

The 1-dimensional likelihood functions suggest that anomalous couplings have been observed at about the 90% confidence level, with a values of $\lambda_\gamma = -0.001$ and $\Delta\kappa_\gamma = -0.02$ preferred by the ‘mock’ data. The P_γ^T distribution is suspicious, however, because a deficit of ‘data’ seems to be observed at mid to high P^T . A cross check sensitive to QCD corrections, but insensitive to anomalous couplings is required. The recoil of the gauge-boson pair $P_{W\gamma}^T$ is very sensitive to (indeed almost equivalent to) the inclusive jet structure in the event, and so is a natural choice. This distribution is shown in Figure 11, wherein the LO ‘mock’ data has been normalised to the NLO expectation using a constant k -factor. In order to obtain this distribution, the jet veto cut has been removed for the event selection.

This $P_{W\gamma}^T$ distribution has very little sensitivity to anomalous couplings. The change in the expectation from an anomalous $\Delta\kappa_\gamma = 0.2$ (already excluded by LEP) and $\lambda_\gamma = 0.01$ (large by LHC standards) are superimposed,¹² and are nearly indistinguishable from the Standard Model expectation.

The ‘mock’ data differs significantly from the model expectation. Since the distribution has essentially no sensitivity to anomalous couplings, the difference arises elsewhere.

As a second example illustrating how the $P_{W\gamma}^T$ distribution can be used to validate the QCD parameters chosen for the reference histograms, the effect of a factor 2 change in the factorisation and renormalisation scales is shown for the $P_{W\gamma}^T$ distribution in Figure 12. In this example both reference and ‘mock’ data histograms are generated at NLO, but the data employs a fixed factorisation scale equal to the W -mass for all events. The reference uses a fixed factorisation scale of two times the W -mass. The ‘mock’ data points are systematically higher than the reference model in the $P^T < 400 \text{ GeV}$ region. The points differ from the model by an amount that cannot be accounted for by the anomalous couplings alone.

In this manner the $P_{W\gamma}^T$ distribution (with jet veto cuts relaxed) may be used in hadron collider experiments to evaluate the ability of the theory to model the data. A good fit between the Monte Carlo and the data for this distribution should first be achieved before attempting to extract anomalous couplings. Since this distribution is primarily sensitive to QCD effects, improvements in the fit may be achieved by tuning the parton density functions, varying the factorization scale, and adjusting the QCD coupling.

There are other regions of phase space which also exhibit a reduced sensitivity to anomalous couplings, and so could be used to validate Monte Carlo modelling independently of the anomalous couplings. The regions include rapidities far from the radiation zero $|\eta_\gamma - \eta_{|W}| > 1.5$, and the low gauge-boson transverse momentum region, where the gauge-boson transverse momentum can be dis-entangled from the inclusive subprocess transverse momentum by requiring that $P_\gamma^T < 200 \text{ GeV}$ in the frame where the $W\gamma$ system has been boosted in the transverse direction such that $P_{W\gamma}^T = 0$.

F. Limits as a Function of Integrated Luminosity

The confidence intervals for the anomalous TGC parameters are limited primarily by statistics. Table X shows confidence intervals for the anomalous TGC parameters for data samples of $\mathcal{L} = 10, 30, 100, 300, 1000, \text{ and } 10^6 \text{ fb}^{-1}$ at the LHC. The spread in the confidence intervals

¹² The confidence limits obtainable at LHC from the $P_{W\gamma}^T$ distribution have already been excluded by LEP.

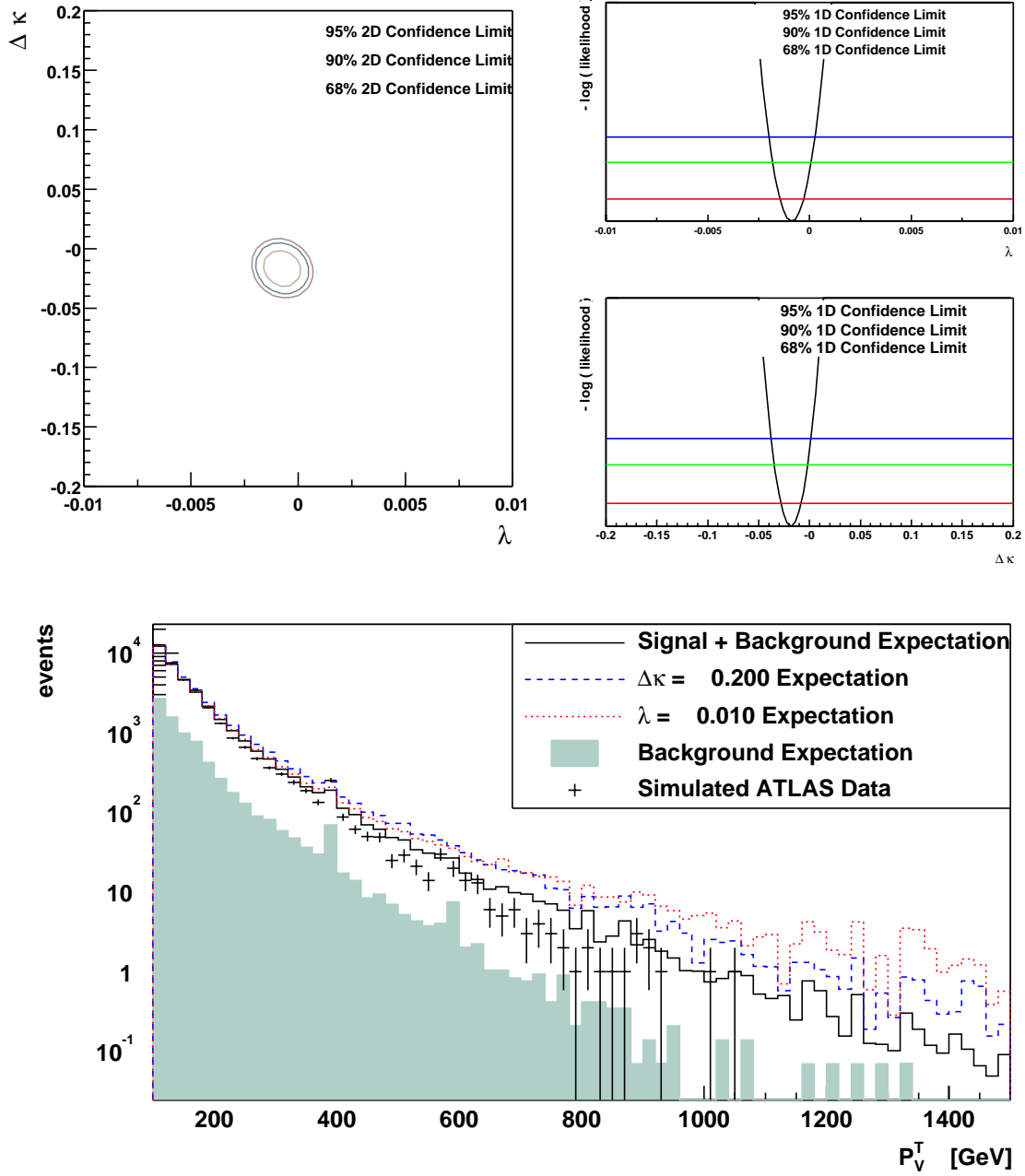


FIG. 10: Differences arising from a mis-modelling of QCD effects are presented. The reference histograms are generated using the BHO NLO generator, while the data is generated using the Pythia LO Monte Carlo. The 2-dimension (top left) and 1-dimension (top right) confidence intervals for λ_γ and $\Delta\kappa_\gamma$ are extracted from the P_γ^T distribution (bottom) using an integrated luminosity of 100 fb^{-1} .

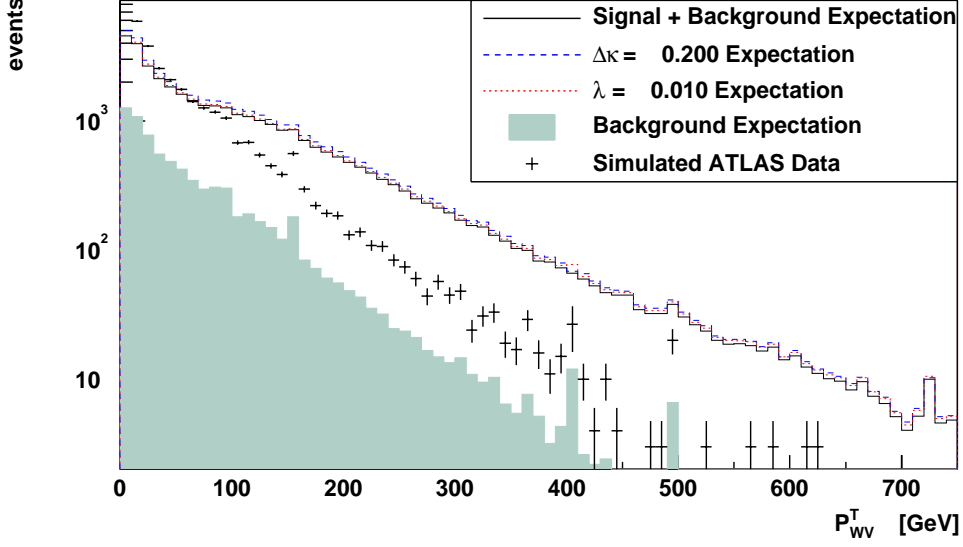


FIG. 11: The distribution of gauge-boson-pair transverse momentum is shown for reference histograms generated using the BHO NLO generator, and the ‘mock’ data generated using the Pythia LO Monte Carlo for an integrated luminosity of 100 fb^{-1} . The LO ‘mock’ data has been normalised to the NLO expectation.

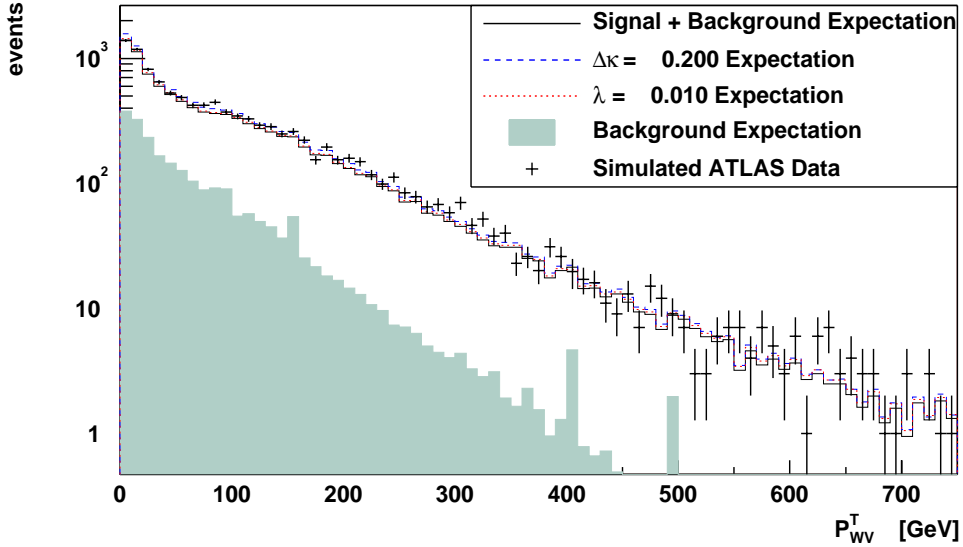


FIG. 12: Differences in the $P_{W\gamma}^T$ distribution arising from a factor two change in the QCD factorization scale are presented for an integrated luminosity of 30 fb^{-1} . Both data and reference histograms are generated at NLO, but the data uses a fixed scale M_W , while the reference uses $2 M_W$.

	95% Statistical Limit	\oplus All Systematics	95% Confidence Limit (stat \oplus syst)
Integrated Luminosity = 10 fb ⁻¹			
P_γ^T	-0.00476 < λ < 0.00486 λ spread= 0.00962	(-0.00119, 0.00117)	-0.00491 < λ < 0.00499 λ spread= 0.00991
P_γ^T	-0.101 < $\Delta\kappa$ < 0.104 $\Delta\kappa$ spread= 0.206	(-0.015, 0.00756)	-0.103 < $\Delta\kappa$ < 0.105 $\Delta\kappa$ spread= 0.207
Integrated Luminosity = 30 fb ⁻¹			
P_γ^T	-0.00328 < λ < 0.0033 λ spread= 0.00657	(-0.00119, 0.00117)	-0.00349 < λ < 0.0035 λ spread= 0.00698
P_γ^T	-0.0732 < $\Delta\kappa$ < 0.0761 $\Delta\kappa$ spread= 0.149	(-0.015, 0.00756)	-0.0747 < $\Delta\kappa$ < 0.0764 $\Delta\kappa$ spread= 0.151
Integrated Luminosity = 100 fb ⁻¹			
P_γ^T	-0.00218 < λ < 0.00218 λ spread= 0.00436	(-0.00119, 0.00117)	-0.00248 < λ < 0.00247 λ spread= 0.00496
P_γ^T	-0.052 < $\Delta\kappa$ < 0.0545 $\Delta\kappa$ spread= 0.106	(-0.015, 0.00756)	-0.0541 < $\Delta\kappa$ < 0.055 $\Delta\kappa$ spread= 0.109
Integrated Luminosity = 300 fb ⁻¹			
P_γ^T	-0.00154 < λ < 0.00149 λ spread= 0.00303	(-0.00119, 0.00117)	-0.00195 < λ < 0.00189 λ spread= 0.00384
P_γ^T	-0.0379 < $\Delta\kappa$ < 0.0403 $\Delta\kappa$ spread= 0.0782	(-0.015, 0.00756)	-0.0407 < $\Delta\kappa$ < 0.041 $\Delta\kappa$ spread= 0.0817
Integrated Luminosity = 1000 fb ⁻¹			
P_γ^T	-0.00106 < λ < 0.000973 λ spread= 0.00204	(-0.00119, 0.00117)	-0.0016 < λ < 0.00152 λ spread= 0.00312
P_γ^T	-0.0266 < $\Delta\kappa$ < 0.0286 $\Delta\kappa$ spread= 0.0552	(-0.015, 0.00756)	-0.0305 < $\Delta\kappa$ < 0.0296 $\Delta\kappa$ spread= 0.0601
Integrated Luminosity = 10 ⁶ fb ⁻¹			
P_γ^T	-0.000101 < λ < 9.93e-05 λ spread= 0.0002	(-0.00119, 0.00117)	-0.00119 < λ < 0.00117 λ spread= 0.00237
P_γ^T	-0.00235 < $\Delta\kappa$ < 0.00255 $\Delta\kappa$ spread= 0.00491	(-0.015, 0.00756)	-0.0152 < $\Delta\kappa$ < 0.00798 $\Delta\kappa$ spread= 0.0232

TABLE X: The 95% confidence intervals for anomalous TGC parameters as a function of integrated luminosity for W_γ production at the LHC.

are shown graphically in Figure 13. These results should be interpreted with caution, because they have been derived by simply scaling the histograms which were constructed to study the sensitivity of the ATLAS experiment for low luminosity LHC running and changes in effects like pile-up have not been accounted for. Nevertheless, the results provide a valuable indication of how an increase in luminosity will improve the sensitivity to anomalous TGC's. The ATLAS experiment is expected to collect 30 fb⁻¹ at low luminosity and 300 fb⁻¹ at high luminosity. The confidence intervals for 1000 and 10⁶ fb⁻¹ are included for interest only, and do not represent expectations for ATLAS.

Confidence intervals for the λ_γ and $\Delta\kappa_\gamma$ parameters are dominated by statistics for integrated luminosities up to at least 300 fb⁻¹, meaning the confidence limits for both parameters will

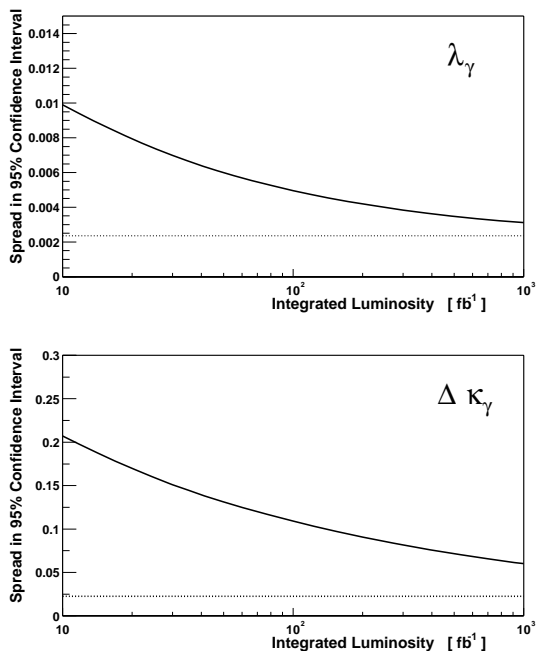


FIG. 13: The 95% confidence intervals (solid lines) are shown as a function of integrated luminosity for $W\gamma$ production at the LHC. The dotted lines indicate the magnitude of the systematic contributions, which are added in quadrature to the 95% statistical confidence limits to obtain the total confidence intervals (shown as solid lines).

always be statistically limited at the LHC experiments. This is because the sensitivity is derived from those events at the highest transverse momentum, such that the measurement relies on just a few of these high P_γ^T events, regardless of the total diboson event rate.

G. Limits as a Function of Form Factor Scale and Mass Scale

Any measurement of anomalous TGC's integrated over a range of diboson invariant mass (which is equivalent to parton centre-of-mass at leading order) depends on the form factor assumptions, as described in Sec. IID. For the results presented thus far, the anomalous TGC's are assumed constant (i.e. $\Lambda_{\text{FF}} = \infty$). In this section, the effect of introducing a dipole form factor (which is the conventional form factor assumption) is studied, and the impact on the confidence intervals is evaluated. After showing that the constant form factor limits at LHC are consistent with the limits that would be obtained with a unitarity-safe dipole form factor, a new strategy of presenting the limits as a function of a diboson mass cutoff is presented.

The form factor scale Λ_{FF} acts as a cutoff on the effects of the anomalous TGC parameters. As such, a smaller Λ_{FF} will result in a reduced impact of the anomalous TGC parameters, making their effect more difficult to observe. As the Λ_{FF} scale assumed in an analysis is increased from a small scale to a larger scale, the confidence intervals will decrease, until eventually an asymptotic limit is reached. This asymptotic limit occurs when the Λ_{FF} is so large that the form factor is operating at a scale at which the experimental data has no sensitivity. In this way, the point at which the limits turn asymptotic reflects the maximum scale at which the experiment is able to probe new physics which has been integrated out using the parametrised TGC Lagrangian. In a previous study of form factors [43], the Λ_{FF} scale at which the limits turn asymptotic was labelled Λ_{machine} , and it was argued that Λ_{machine} is a property of the collider machine, and the most natural choice for a dipole form factor scale in the case where confidence limits are being derived. This strategy was adopted in Refs. [8] and [44], and is the natural strategy for dipole form factors.

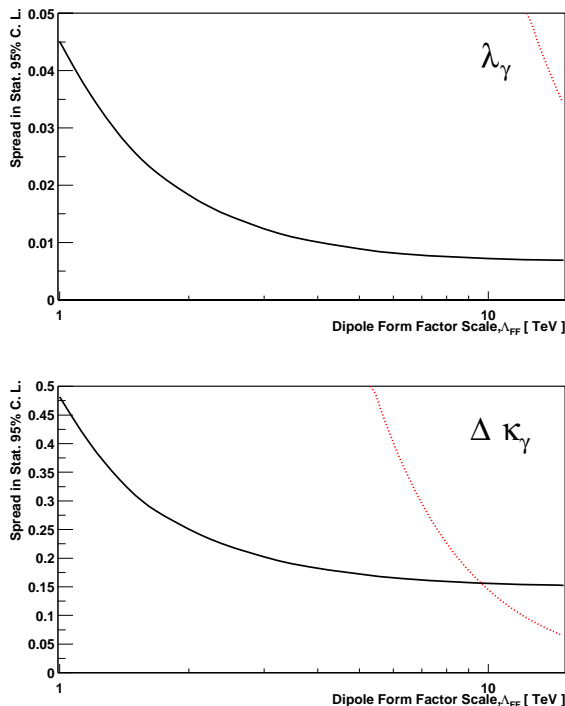


FIG. 14: The spread in statistical 95% confidence intervals (solid lines) are shown as a function of the dipole form factor scale assumption Λ_{FF} for $W\gamma$ production at the LHC. The dotted lines indicate the approximate Born level unitarity limits from Eq. 8. The region above the solid line is excluded by the experiment, while the region to the right of the dotted line is excluded by unitarity.

The spread in the statistical 95% confidence limits are presented in Figure 14 as a function of form factor scale Λ_{FF} , assuming the dipole ($n=2$) form factor expression of Eq. 7. The limits turn asymptotic at about $\Lambda_{\text{machine}} = 5$ to 10 TeV. Increasing Λ_{FF} beyond this value will not improve the anomalous TGC limits. This implies TGC measurements at the LHC are able to probe new physics operating at a scale up to about 5 or 10 TeV. The unitarity limits (as presented in Eq. 8) are superimposed on the plots as dotted lines.

For the limits presented in this paper, constant anomalous TGC's have been used, which is equivalent to $\Lambda_{\text{FF}} = \infty$, and violates unitarity at high energy scales. Figure 14 can be used to evolve these limits back to any dipole form factor scale choice. From the figure, one may see that the $\Lambda_{\text{FF}} = \infty$ form factor scale provides equivalent results down to scales of about 5 TeV. This is Λ_{machine} for $WW\gamma$ couplings at the LHC.

Before discussing the approach for presenting the limits as a function of mass scale, a few comments are in order about the choice of scale for a dipole form factor. The authors advocate against an approach which uses a form factor scale which is significantly smaller than Λ_{machine} (5 to 10 TeV at the LHC, and about 2 TeV at the Tevatron) and prefers to present limits using Λ_{machine} even if those limits would be in violation of unitarity. The primary argument in support of this philosophy is that the Λ_{FF} defines the scale at which the effective Lagrangian description (wherein the new physics has been integrated out and described in terms of a small number of low-dimensional operators) breaks down. Effectively, a scale has been reached at which the effects of the new physics are directly visible. There is no reason to expect the effects of this new physics to turn off at that scale—rather it will appear directly, but will not be parameterisable in terms of the effective TGC Lagrangian. If a form factor scale smaller than Λ_{machine} is used, then it will be absolutely essential to *neglect data* collected at the scales where the assumed form factor operates. This is because in that energy regime, the effective model Lagrangian is fully constrained to the Standard Model (since the anomalous TGC's $\rightarrow 0$ at

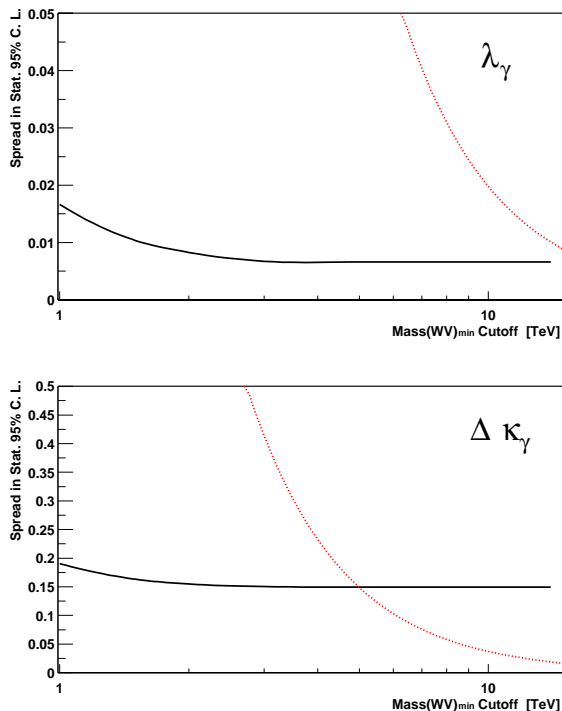


FIG. 15: The spread in statistical 95% confidence intervals (solid lines) are shown for $W\gamma$ production as a function the diboson mass cutoff, which is used as a selection criteria for events included in the analysis. The dotted lines indicate the approximate Born level unitarity limits from Eq. 6. An integrated luminosity of 30 fb^{-1} at the LHC has been assumed. The region above the solid line is excluded by the experiment, while the region to the right of the dotted line is excluded by unitarity.

Λ_{FF}), and it makes no sense to include such data in a fit to extract the anomalous TGC's.¹³ However, the data which is collected at the largest scales is potentially the most interesting, and one does not wish to be in a position where it needs to be discarded.

In Figure 15 a different method for reporting the limits is presented. Here the limits are presented as a function of a diboson mass cutoff (the minimum mass solution of Eq. A.21 is used). For example, the limits at $\text{Mass}(W\gamma)_{\text{min}} = 2 \text{ TeV}$ use only the data for which the reconstructed minimum mass solution is less than 2 TeV. As for the dipole form factor scale, an asymptotic limit is reached. This time it occurs at about 3 TeV. The unitarity limit is superimposed on the plots as a dotted line (here the unitarity limits of Eq. 6 are the relevant ones). The region above the solid line is excluded by the experiment, while the region to the right of the dotted line is excluded by unitarity.

This strategy allows for the presentation of limits without introducing arbitrary choices for the energy dependent form factor parametrisation. It shows the ultimate reach of the experiment, while allowing the interpretation of the results at any mass scale. Further, if an anomalous coupling ‘turns on’ or ‘turns off’ at some mass scale, that would be reflected in the limits.

In summary, the use of a specific energy dependent form factor parametrisation in the effective TGC Lagrangian is arbitrary, and contrary to the underlying assumption of being able to integrate out the physics which is producing the anomaly. Rather than safeguarding unitarity by invoking these form factors, we advocate presenting the confidence intervals as a function of a diboson mass cutoff which is applied to the data. The point where these limits

¹³ The danger of performing such a fit is demonstrated by an example in Ref. [43], wherein it was shown that a measurement of a small anomalous TGC parameter which is constant at scales $\leq \Lambda_{\text{machine}}$ will be vastly over-estimated if a form factor scale smaller than Λ_{machine} is artificially imposed.

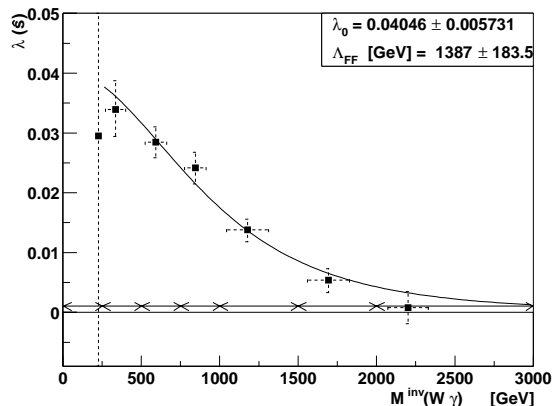


FIG. 16: Measurement of the λ_γ parameter as a function of energy is demonstrated using 30 fb^{-1} integrated luminosity for LHC $W\gamma$ production. The ‘mock’ ATLAS data has been generated with $\lambda_{\gamma_0}=0.04$ using a dipole form factor of scale $\Lambda_{\text{FF}} = 1500 \text{ GeV}$. The solid line is a fit to Λ_{FF} and the bare coupling λ_{γ_0} assuming the dipole form factor. The arrows along the x -axis indicate the diboson mass bin widths.

turn asymptotic is a measure of the ultimate reach of the experiment. These limits provide information about the anomalous TGC’s in a manner which is as free as possible from arbitrary assumptions.

H. Measuring the Energy Dependence of Anomalous TGC’s

The form factor discussion of the previous section raises the question which has been posed in Ref. [45]: if anomalous TGC measurements at LHC are inconsistent with the Standard Model, is it possible to measure the energy dependence (i.e. form factor behaviour) of the anomalous TGC parameters? The feasibility of such a measurement at hadron colliders has been demonstrated in Refs. [8, 43]. In this section, energy dependent measurements of anomalous TGC’s are explored.

A large data sample of diboson events will be necessary to perform such a measurement, because the data needs to be separated out into bins of diboson mass. For $W\gamma$ production, this is complicated by the two-fold ambiguity in reconstructing the diboson invariant mass. In the appendix of this paper, the M_{Min} solution (c.f. Eq. A.21) is shown to be a good estimator of the true diboson mass. This is the diboson mass estimator which is used here to divide the events into energy bins. For each diboson mass bin, the anomalous TGC parameters can be estimated using any of the techniques of Sec. VB. In this case, no form factor should be imposed on the reference distributions, since it is this form factor which is being measured. For this study the anomalous TGC’s have been estimated in each bin using a maximum likelihood fit to the P_γ^T distribution.

To demonstrate the method, ‘mock’ ATLAS data has been generated with bare coupling $\lambda_{\gamma_0} = 0.04$ and a dipole ($n=2$) form factor¹⁴ with $\Lambda_{\text{FF}} = 1500 \text{ GeV}$. This ‘mock data’ is then compared to reference histograms of the bare coupling λ_{γ_0} (i.e. the reference histograms do not use a form factor) for each of the diboson mass bins. The results are presented in Figure 16. The events have been separated out into diboson mass bins ranging from 250 GeV to 3000 GeV with variable width, to ensure adequate statistics in each bin. Since the distribution of events within each bin is not uniform, the measured value for λ_{γ_0} inside each bin is indicated at the location of the mean diboson mass for the events inside the bin. The behaviour of the couplings

¹⁴ i.e. the coupling is $\lambda_\gamma = \lambda_{\gamma_0} / (1 + \frac{M_{W\gamma}^2}{\Lambda_{\text{FF}}^2})^2$.

as a function of energy is clearly visible. A fit to the dipole form factor function is also indicated with a solid line. The parameters which were used to generate the ‘mock’ data are reproduced within the precision of the fit.

The relatively large event rate and sensitivity to the anomalous TGC couplings for $W\gamma$ production makes measurements of the λ_γ parameter feasible with as little as 10 fb^{-1} of data. Measurements of the $\Delta\kappa_\gamma$ parameter requires more data, and will likely not be feasible at the LHC with precisions that have not already been excluded by LEP and Tevatron data.

VI. CONCLUSIONS

The LHC provides an ideal environment for testing the Standard Model through the self interactions of gauge-bosons by measuring the triple gauge-boson couplings (TGC’s) which parametrise in a generic way the interactions between three gauge-bosons. This study focuses on the measurement of $WW\gamma$ couplings through the $W\gamma$ production mechanism, with the W -boson decaying to electron and muon type leptons.

The analysis is optimised for proton-proton collisions at 14 TeV and a luminosity of $10^{33} \text{ cm}^{-2} \text{ s}^{-1}$, which corresponds to the low luminosity running period at the LHC. An integrated luminosity of 30 fb^{-1} has been assumed for all of the results. W +jet production with the jet misidentified as a photon is the most important background. The $W(\rightarrow \tau\nu), \gamma$ channel is an important irreducible background.

The radiation zero refers to a particular emission angle of the photon in $W\gamma$ production which is forbidden by subtle gauge cancellations. The radiation zero has yet to be observed experimentally. The effect will be clearly observable with 30 fb^{-1} of data from the LHC, and the characteristic asymmetric shape can be observed with symmetric proton-proton collisions by ‘signing’ the rapidity separation distribution according to the boost of the γ, l_W^\pm system.

In the scenario where the anomalous TGC parameters are consistent with the Standard Model, the LHC experiments will be in a position to set confidence limits on the anomalous parameters. A maximum likelihood fit to the transverse momentum of the photon (P_γ^T) has been the conventional method for extracting the confidence intervals. It has been compared to several other methods, including a number of other one and two dimension distributions, and the P_γ^T distribution remains the best means of extracting the couplings for most of the TGC parameters. The two dimensional distribution of P_γ^T versus the transverse momentum of the charged lepton from the W -decay is also very effective. The expected 95% confidence intervals for anomalous couplings are

$$\begin{aligned} -0.0033_{\text{stat.}}, \quad -0.0012_{\text{syst.}} &< \lambda_\gamma < \quad +0.0033_{\text{stat.}}, \quad +0.0012_{\text{syst.}} \\ -0.073_{\text{stat.}}, \quad -0.015_{\text{syst.}} &< \Delta\kappa_\gamma < \quad +0.076_{\text{stat.}}, \quad +0.0076_{\text{syst.}} \end{aligned}$$

using 30 fb^{-1} (about 3 years) of low luminosity LHC data.

For all of the anomalous TGC parameters, the confidence intervals will be dominated by statistics throughout the lifetime of the LHC. The theoretical modelling of higher order QCD effects is the dominant systematic. The distribution of the recoil of the gauge-bosons $P_{W\gamma}^T$, is a useful tool for understanding and correcting these effects because the distribution is highly sensitive to QCD corrections, but is not sensitive to anomalous TGC’s at a level which has not already been excluded by previous experiments (LEP and Tevatron). A comparison of data to simulation using this distribution will provide an important cross-check that higher order corrections have been properly modelled when measuring TGC’s at the LHC.

Dipole form factors have been the conventional means of guaranteeing unitarity in the TGC Lagrangian. The parametrisation of the form factors is arbitrary, and introduces unnecessary dependence on the parametrisation choice into the experimental results. Though the confidence intervals as a function of a dipole form factor parametrisation have been included in this study, it has been argued here that it is preferable to report the limits as a function of a diboson invariant mass cutoff which is applied to the data. The LHC data will directly probe diboson invariant mass scales up to about 3 TeV, which is the scale at which the limits as a function of the mass cutoff turn asymptotic. Since unitarity is violated only for diboson mass cutoffs above 3 TeV, the limits reported here are unitarity safe, and are presented without any cutoff or form factor.

In the scenario where non-standard anomalous TGC parameters are observed, the LHC event rate will be sufficiently large to bin the data according to the diboson invariant mass. The couplings can then be measured separately in each of these bins so as to observe the energy dependent (i.e. form factor) behaviour of the couplings, without assuming a particular form factor parametrisation.

Acknowledgements

We have benefited from discussions with Jorgen Beck Hansen and Samira Hassani. We are grateful to Ulrich Baur for informative correspondence, comments, and discussions. This work has been supported by the Natural Sciences and Engineering Research Council of Canada.

-
- [1] R. Barate *et al.* [ALEPH Collaboration], “Measurement of W pair production in e^+e^- collisions at 183 GeV,” *Physics Letters B* **453**, 107 (1999) [hep-ex/9903053].
 - [2] P. Abreu *et al.* [DELPHI Collaboration], “ W pair production cross-section and W branching fractions in e^+e^- interactions at 183 GeV,” *Physics Letters B* **456**, 310 (1999).
 - [3] M. Acciarri *et al.* [L3 Collaboration], “Measurement of W pair cross sections in e^+e^- interactions at $\sqrt{s} = 183$ GeV and W decay branching fractions,” *Physics Letters B* **436**, 437 (1998).
 - [4] G. Abbiendi *et al.* [OPAL Collaboration], “ W^+W^- production and triple gauge boson couplings at LEP energies up to 183 GeV,” *European Physical Journal C* **8**, 191 (1999) [hep-ex/9811028].
 - [5] D. Fouchez, “Gauge boson pairs production study with Atlas”, ATLAS Internal Note PHYS-NO-060, 24 November, 1994.
 - [6] J.B. Hansen, “Triple Gauge-boson Couplings in Boson Pair Production”, presented at the ATLAS Physics Week in Grenoble April 1998.
 - [7] M. Dobbs and M. Lefebvre, “Prospects for Probing the Three Gauge-boson Couplings in $W + Z$ Production at the LHC”, ATLAS Internal Note, ATL-COM-PHYS-2002-020, 2002.
 - [8] S. Hassani, “Prospects for Measuring Neutral Gauge Boson Couplings in ZZ Production with the ATLAS Detector”, ATLAS Internal Communication ATL-COM-PHYS-2002-012, 2002;
S. Hassani, “Prospects for Measuring Neutral Gauge Boson Couplings in $Z\gamma$ Production with the ATLAS Detector”, ATLAS Internal Communication ATL-COM-PHYS-2002-013, 2002.
 - [9] K. Hagiwara, R. D. Peccei, D. Zeppenfeld and K. Hikasa, “Probing the Weak Boson Sector in $e^+e^- \rightarrow W^+W^-$,” *Nuclear Physics B* **282**, 253 (1987).
 - [10] D. Zeppenfeld and S. Willenbrock, “Probing the Three Vector-Boson Vertex at Hadron Colliders,” *Physical Review D* **37**, 1775 (1988).
 - [11] U. Baur and D. Zeppenfeld, “Probing the $WW\gamma$ Vertex At Future Hadron Colliders,” *Nuclear Physics B* **308**, 127 (1988).
 - [12] H. Aihara, T. Barklow, U. Baur, J. Busenitz, S. Errede, T.A. Fuess, T. Han, D. London, J. Ohnemus, R. Szalapski, C. Wendt, D. Zeppenfeld, “Anomalous gauge boson interactions”, Summary of

- the Working Subgroup on Anomalous Gauge Boson Interactions of the DPF Long-Range Planning Study, published in *Electroweak Symmetry Breaking and Beyond the Standard Model*, eds. T. Barklow, S. Dawson, H. Haber and J. Seigrist, LBL-37155, March 1995, 53 pages [hep-ph/9503425].
- [13] K. O. Mikaelian, “Photoproduction of Charged Intermediate Vector Bosons,” *Physical Review D* **17**, 750 (1978);
 R. W. Brown, D. Sahdev and K. O. Mikaelian, “ $W^\pm Z^0$ and $W^\pm \gamma$ Pair Production in νe , pp , $\bar{p}p$ Collisions,” *Physical Review D* **20**, 1164 (1979);
 K. O. Mikaelian, M. A. Samuel and D. Sahdev, “The Magnetic Moment of Weak Bosons Produced in pp and $\bar{p}p$ Collisions,” *Physical Review Letters* **43**, 746 (1979).
- [14] U. Baur, T. Han and J. Ohnemus, “Amplitude zeros in $W^\pm Z$ production,” *Physical Review Letters* **72**, 3941 (1994) [hep-ph/9403248].
- [15] U. Baur, R.K. Ellis, and D. Zeppenfeld (Editors), “QCD and Weak Boson Physics in Run II” Workshop Proceedings, March–November 1999, FERMILAB-PUB-00-297 (November 2000).
- [16] P. Fisher, U. Becker and J. Kirkby, “Very high precision tests of the electroweak theory,” *Physics Letters B* **356**, 404 (1995).
- [17] U. Baur, S. Keller and W. K. Sakumoto, “QED radiative corrections to Z boson production and the forward backward asymmetry at hadron colliders,” *Physical Review D* **57**, 199 (1998) [hep-ph/9707301].
- [18] U. Baur, T. Han and J. Ohnemus, “QCD corrections to hadronic $W\gamma$ production with nonstandard $WW\gamma$ couplings,” *Physical Review D* **48**, 5140 (1993).
- [19] U. Baur, T. Han and J. Ohnemus, “ WZ production at hadron colliders: Effects of nonstandard WWZ couplings and QCD corrections,” *Physical Review D* **51**, 3381 (1995) [hep-ph/9410266].
- [20] U. Baur, D. Zeppenfeld, “Unitarity Constraints on the Electroweak Three Vector Boson Vertices,” *Physics Letters B* **201**, 383 (1988).
- [21] U. Baur, T. Han and J. Ohnemus, “QCD corrections and nonstandard three vector boson couplings in W^+W^- production at hadron colliders,” *Physical Review D* **53**, 1098 (1996) [hep-ph/9507336].
- [22] The LEP Collaborations Aleph, Delphi, L3, OPAL and the Electroweak Working Group, “A combination of preliminary electroweak measurements and constraints on the standard model,” hep-ex/0103048, March 2001.
- [Sjö01b] T. Sjöstrand, L. Lönnblad and S. Mrenna, “Pythia 6.2 User Manual” LU TP 01-21, [hep-ph/0108264], 2001.
- [23] J. Ohnemus and J. F. Owens, “An Order α_S Calculation of Hadronic ZZ Production,” *Physical Review D* **43**, 3626 (1991);
 J. Ohnemus, “An Order α_S calculation of hadronic W^-W^+ production,” *Physical Review D* **44**, 1403 (1991);
 J. Ohnemus, “An Order α_S calculation of hadronic $W^\pm Z$ production,” *Physical Review D* **44**, 3477 (1991);
 J. Ohnemus, “Order α_S calculations of hadronic $W^\pm \gamma$ and $Z\gamma$ production,” *Physical Review D* **47**, 940 (1993).
- [24] L. J. Bergmann, *Next-to-leading-log QCD calculation of symmetric dihadron production*, Ph.D. thesis, Florida State University, 1989;
 H. Baer, J. Ohnemus and J. F. Owens, “A Next-to-Leading Logarithm Calculation of Jet Photoproduction,” *Physical Review D* **40**, 2844 (1989).
- [25] H. Baer, J. Ohnemus and J. F. Owens, “A Next-to-Leading Logarithm Calculation of Jet Photoproduction,” *Physical Review D* **40**, 2844 (1989).
- [26] M. Dobbs, “Partonic Simulation Tools for Diboson Production”, contribution to S. Haywood *et al.* “Electroweak Physics”, in the *Proceedings of the Standard Model Physics (and more) at the LHC Workshop*, Geneva, 1999, CERN-TH-2000-102 [hep-ph/0003275].
- [27] R. K. Ellis, W. J. Stirling and B. R. Webber, “QCD and Collider Physics,” Cambridge Monographs in Particle Physics, Nuclear Physics and Cosmology **8**, 1 (1996).
- [28] T. Sjöstrand, P. Eden, C. Friberg, L. Lönnblad, G. Miu, S. Mrenna and E. Norrbin, “High-energy-physics event generation with PYTHIA 6.1,” *Computer Physics Communications* **135**, 238 (2001) [hep-ph/0010017].
- [29] H. L. Lai *et al.*, “Improved parton distributions from global analysis of recent deep inelastic scat-

- tering and inclusive jet data,” *Physical Review D* **55**, 1280 (1997) [hep-ph/9606399].
- [30] E. Richter-Was, D. Froidevaux, and L. Poggioli, “ATLFAST 2.0 a fast simulation package for ATLAS”, ATLAS Internal Communication ATL-PHYS-98-131, 1998.
 - [31] The ATLAS Collaboration, *ATLAS Detector and Physics Performance Technical Design Report*, CERN/LHCC/99-14 and CERN/LHCC/99-15, 25 May 1999.
 - [32] M. Wieler, “Photon Identification with the ATLAS Detector”, ATLAS Internal Note ATL-PHYS-99-016, 1999.
 - [33] M. Wieler, “Isolation of Photons”, ATLAS Internal Communication ATL-COM-PHYS-2001-024, 2001.
 - [34] P. Pralavorio, “Electron/Jet Separation with the ATLAS Detector”, ATLAS Internal Note ATL-PHYS-99-015, 1999.
 - [35] The ATLAS Collaboration, *ATLAS Technical Proposal*, CERN/LHCC/94-43, 15 December 1994.
 - [36] M. Kelly [D0 Experiment], “Test of the standard model of electroweak interactions by measuring the anomalous $WW\gamma$ coupling at $\sqrt{s} = 1.8$ TeV”, Notre Dame Ph.D. Thesis, South Bend Indiana, 1996.
 - [37] Catherine K. Mackay, *The Electromagnetic Calorimeter for CMS and a Study of the $WW\gamma$ Vertex*, Ph.D. Thesis, Brunel University, September 1998 [CMS 1999/012 THESIS];
C. K. Mackay, “Observing Anomalous Di-Boson Couplings in the $WW\gamma$ Vertex at CMS”, CMS NOTE-2001/052;
C. K. Mackay, “Sensitivity of CMS to CP Conserving Anomalous Di-Boson Couplings in $W\gamma$ Events”, CMS NOTE-2001/056.
 - [38] E. Barberio and Z. Was, “PHOTOS: A Universal Monte Carlo for QED radiative corrections. Version 2.0,” *Computer Physics Communications* **79**, 291 (1994).
 - [39] J. Alitti *et al.* [UA2 Collaboration], “Direct measurement of the $W\gamma$ coupling at the CERN $\bar{p}p$ collider,” *Physics Letters B* **277**, 194 (1992).
 - [40] M. Dobbs, “Phase space veto method for next-to-leading order event generators in hadronic collisions”, *Physical Review D* **65**, 094011 (2002), [hep-ph/0111234].
 - [41] H. L. Lai *et al.*, “Global QCD analysis and the CTEQ parton distributions,” *Physical Review D* **51**, 4763 (1995) [hep-ph/9410404].
 - [42] M. Diehl and O. Nachtmann, “Optimal observables for the measurement of three gauge boson couplings in $e^+e^- \rightarrow W^+W^-$,” *Zeitschrift für Physik C* **62**, 397 (1994).
 - [43] M. Dobbs, “Unitarity Limits and Form Factors”, contribution to S. Haywood *et al.* “Electroweak Physics”, in the *Proceedings of the Standard Model Physics (and more) at the LHC Workshop*, Geneva, 1999, CERN-TH-2000-102 [hep-ph/0003275].
 - [44] T. Müller, D. Neuberger, W.H. Thuemmel, “Sensitivities for anomalous $WW\gamma$ and $ZZ\gamma$ couplings at CMS”, CMS Internal Note CMS NOTE-2000/017, 2000.
 - [45] G. J. Gounaris, J. Layssac and F. M. Renard, “Signatures of the anomalous $Z\gamma$ and ZZ production at the lepton and hadron colliders,” *Physical Review D* **61**, 073013 (2000) [hep-ph/9910395].
 - [46] D. Benjamin, “ $W\gamma$ and $Z\gamma$ production at the Tevatron,” FERMILAB-CONF-95-241-E *Presented at 10th Topical Workshop on Proton-Antiproton Collider Physics, Batavia, IL, 9-13 May 1995*.
 - [47] D. De Florian and A. Signer, “ $W\gamma$ and $Z\gamma$ production at hadron colliders,” *European Physical Journal C* **16**, 105 (2000) [hep-ph/0002138].
 - [48] M. Dobbs, *Probing the Three Gauge-boson Couplings in 14 TeV Proton-Proton Collisions*, Ph.D Thesis, University of Victoria, 2002.

APPENDIX

Event Reweighting as a Function of Anomalous Couplings

Each event generated by the BHO programs has associated with it a weight, which is a function of the input parameters including the anomalous TGC parameters. In the analysis stage, these events will be combined into histograms. The key requirement for these histograms

is that they must be known as a function of the anomalous TGC parameters. This could be accomplished by dividing the anomalous TGC parameter space into a grid of discrete points, and generating a separate event sample for each point. However, this would complicate the analysis, because differences between two points in the grid could arise not only from the different anomalous TGC parameters, but also from statistical effects owing to the finite number of events in each sample. Since there are 3 (2) anomalous TGC parameters which need to be accounted for in WZ ($W\gamma$) production, the number of event samples necessary would be 3^n (2^n), where n is the number of divisions on the grid. For an accurate description, n would have to be $\mathcal{O}(50)$. Several million events are necessary in each event sample in order to effect the cancellations inherent in the NLO simulation. With present computer technology, the simulation of a single event sample (including hadronization and fast detector simulation), is already a time consuming affair, requiring about a day of computer time. Therefore, this sort of approach would not be feasible in terms of computer time.

A better approach is to modify the BHO programs to provide the event weights as a function of the anomalous TGC parameters. These functions can then be used to reweight the distributions, providing a prediction of the histograms for any choice of the anomalous TGC parameters.

Since the matrix elements are linear functions of the anomalous TGC parameters, the differential cross section (or event weight) is a quadratic function of the parameters. For $W\gamma$ production, there are 2 parameters, λ_γ and $\Delta\kappa_\gamma$, and so the event weight can be written

$$\text{weight}^{W\gamma}(\Delta\kappa_\gamma, \lambda_\gamma) = w_{00} + \Delta\kappa_\gamma w_{0\kappa} + \lambda_\gamma w_{0\lambda} + \lambda_\gamma \cdot \Delta\kappa_\gamma w_{\lambda\kappa} + \Delta\kappa_\gamma^2 w_{\kappa\kappa} + \lambda_\gamma^2 w_{\lambda\lambda}. \quad (\text{A.17})$$

The SM event weight is w_{00} . For WZ production there would be 3 parameters (Δg_Z^1 , λ_Z , $\Delta\kappa_Z$), and therefore 10 w_{ij} weights.

The six w_{ij} weights for $W\gamma$ production can be evaluated for each event by constructing six linearly independent equations from a grid of points in λ_γ , $\Delta\kappa_\gamma$ space, re-evaluating the event weight for the same kinematic configuration at each of the six points, and inverting the resultant matrix equation to solve for the w_{ij} parameters. No form factors are applied to the anomalous TGC's for this procedure. Since interpolation is preferred over extrapolation, the λ_γ , $\Delta\kappa_\gamma$ points are chosen to be considerably larger than the sensitivity expected in the TGC analysis, and the grid is centred on the SM values.

One extra parameter besides the w_{ij} 's needs to be stored with each event in order to allow for the evaluation of the corresponding event weight for arbitrary choices of the anomalous TGC parameters. This parameter is the diboson system invariant mass, which is needed to apply form factors to the anomalous TGC parameters. Together the w_{ij} 's and the diboson invariant mass are referred to here as the *reweighting parameters*.

There is an added complication which arises because of the regularisation scheme which has been used for the NLO matrix elements. The BHO programs employ the 2 parameter phase space slicing method. Events without a coloured emission in the final state include a numerical integration to account for the small amount of coloured emission phase space which has been defined as unresolvable and partitioned into the event weight. There is also a degree of freedom which specifies the gauge-boson polarisations. Thus, two events with identical kinematics might have very different event weights (which is in no way inconsistent with the Monte Carlo method), because only a subset of the phase space degrees of freedom specify the kinematics. This means that for the calculation of the reweighting parameters, one needs to be careful to keep the phase space which specify this additional numerical integration and the gauge-boson polarisations

fixed while re-evaluating the event weights at the linearly independent points on the grid.¹⁵

When the complete phase space (including polarisations and the additional phase space slicing numerical integration) is fixed for the evaluation of the reweighting parameters, the systematic bias which results for an individual event weight is only a few times larger than the computer precision. For an inclusive quantity such as a cross section, the systematic error is many orders of magnitude smaller than the statistical precision.

With the reweighting parameters known for each event, they can be used separately to construct *reweighting histograms* of any experimental observable (e.g. the transverse momentum of one vector boson). For $W\gamma$ production, six separate histograms corresponding to the six weights in Eq. A.17 are used. Reference histograms of the experimental observable can then be obtained for any choice of the anomalous TGC parameters by adding together the reweighting histograms, with each histogram weighted by the appropriate anomalous TGC parameter(s).¹⁶

Reconstructing the Centre-of-Mass System Kinematics

Many of the methods for measuring anomalous TGC parameters which have been discussed in this paper require the reconstruction of the full event kinematics. This section describes the considerations which are important for this reconstruction.

For processes such as $pp \rightarrow Z(\rightarrow l^+l^-)\gamma$ which produce final state particles with directly observable momenta, the centre-of-mass system energy and momentum can be directly inferred from the measured four-vectors. For the leptonic decay channels of hadronic $W^\pm\gamma$ production, a complete reconstruction of the center-of-mass system is made difficult by the presence of an invisible neutrino from the W -decay. Unlike the lepton-collider case, the energy and longitudinal boost of the partons inside the colliding (anti-)protons participating in the hard interaction are unknown, and so their momentum fractions x_a, x_b can only be inferred from the final state particles.

When the final state contains a single invisible neutrino coming from a W^\pm , such as for $pp^{(-)} \rightarrow W^\pm(\rightarrow l^\pm\nu)\gamma$ or $pp^{(-)} \rightarrow W^\pm(\rightarrow l^\pm\nu)Z(\rightarrow l^+l^-)$, then the final state four-vectors and center-of-mass can be reconstructed up to a two-fold ambiguity by making some simple assumptions:

1. assume the missing transverse momentum arises exclusively from the invisible neutrino

$$\vec{P}_\nu^T \equiv \vec{P}_{\text{miss}}^T \quad (\text{A.18})$$

2. assume the W^\pm is on-shell (“on-shell W -mass constraint”)

$$(P_\nu + P_{l_W^\pm})^2 \equiv M_W^2. \quad (\text{A.19})$$

The first constraint removes the degrees of freedom associated with the neutrino transverse directions, while the second constraint maps the neutrino longitudinal momentum degree of freedom onto the W -mass degree of freedom. With these assumptions, there are two neutrino

¹⁵ This effect may be responsible for the rather large systematic error which has been associated with this type of cross section parametrisation in previous studies. For example, a 2% error was specified in Ref. [37].

¹⁶ If form factors are applied, they must be included when the reweighting histograms are created, because the form factors are different for each event. This means that the reweighting histograms would have to be recreated any time the form factor parametrisation is changed.

momentum solutions. They can be calculated by enforcing four-momentum conservation, and are given by

$$\begin{aligned}
 P_\nu^x &= P_{\text{miss}}^x \\
 P_\nu^y &= P_{\text{miss}}^y \\
 P_\nu^z &= \frac{1}{2P_{l_W^\pm}^T} \left[P_{l_W^\pm}^z \left(M_W^2 + 2\vec{P}_{l_W^\pm}^T \cdot \vec{P}_\nu^T \right) \pm |\vec{P}_{l_W^\pm}| \sqrt{\left(M_W^2 + 2\vec{P}_{l_W^\pm}^T \cdot \vec{P}_\nu^T \right)^2 - 4P_{l_W^\pm}^T{}^2 P_{\text{miss}}^T{}^2} \right]
 \end{aligned}
 \tag{A.20}$$

where l_W^\pm is the charged lepton from the W -decay.

The two-fold ambiguity arising in the reconstruction of the neutrino longitudinal momentum results in two solutions for the $W\gamma$ system mass,¹⁷ $M_{W\gamma}$. When extracting anomalous coupling limits, this has no profound consequence aside from a reduction in sensitivity since the effect of the ambiguity is easily accounted for by also including the wrong-solutions in the reference Monte Carlo distributions to which the experimental data is compared.

The situation is different when attempting to measure the energy dependence of anomalous couplings. For on-shell diboson production, the relevant scale for the TGC vertex is the $W\gamma$ system invariant mass, and so the measurement of anomalous couplings as a function of $M_{W\gamma}$ will be the goal. This is made difficult by the existence of two mass solutions ($M_{\text{Sol1}}, M_{\text{Sol2}}$) for each event. Of the two solutions, one may be considered the truth solution, M_{Truth} and the other the incorrect solution $M_{\text{WrongSolution}}$. Experimentally there is no way to ascertain which solution is the truth, and so M_{Truth} and $M_{\text{WrongSolution}}$ are not observable quantities. However, with a Monte Carlo simulation, the correct solution is known, and so the simulation may be used to evaluate an effective estimator for M_{Truth} .

For proton-antiproton collisions (such as at the Tevatron), the valence quarks dominate the interaction and the radiation zero conspires with the structure functions to give a preferred direction for P_ν^z . The correct solution may be obtained 73% of the time by simply choosing the forward (i.e. $\max(P_{\nu_{\text{Sol1}}}^z, P_{\nu_{\text{Sol2}}}^z)$) neutrino solution for $W^+\gamma$ production, and the backward ($\min(P_{\nu_{\text{Sol1}}}^z, P_{\nu_{\text{Sol2}}}^z)$) neutrino solution for $W^-\gamma$ production [46]. The situation is different for symmetric pp beam colliders such as the LHC.

The diboson production differential cross section falls exponentially with increasing $M_{W\gamma}$, and so the smaller of the two solutions

$$M_{\text{Min}} = \min(M_{\text{Sol1}}, M_{\text{Sol2}}) \tag{A.21}$$

is more probable. The correlations between M_{Min} and M_{Truth} have been studied in Ref. [47]. The quantities are found to be highly correlated under LHC conditions. However, one might expect the differences to be more pronounced for anomalous TGC confidence limits than in the distributions, since the limits derive a large portion of their sensitivity from the high mass region, and an estimator like M_{Min} is biased towards low masses. A comparison of the difference in sensitivity to anomalous TGC's between M_{Truth} and M_{Min} has been investigated in Ref. [48], wherein the sensitivity of the two distributions is found to be similar (within a few percent).

The average of the two solutions is another estimator. Two definitions may be used for the distribution arising from this estimator, which has caused some confusion in the literature. The

¹⁷ The l^\pm, P_{miss}^T signature arising from a W -decay always has one or two solutions if the momenta are perfectly reconstructed. However, detector resolution effects and the contributions from backgrounds means that in practise there will be many cases in which a l^\pm, P_{miss}^T signature does not have any solution (i.e. the discriminant of Eq. A.20 is negative).

<u>Unobservable</u>	
M_{Truth}	the ‘true’ solution
$M_{\text{WrongSolution}}$	the ‘incorrect’ solution
<u>Reconstructible without assumptions</u>	
(Eq. A.24) M_{Tran}	$(l_W\gamma; P_{\text{miss}}^T)$ cluster transverse (or minimum) mass
<u>Reconstructible with assumptions of Eqs. A.18 and A.19</u>	
	$M_{\text{Sol1}}, M_{\text{Sol2}}$ two solutions from the two-fold ambiguity in neutrino longitudinal momentum, Eq. A.20
(Eq. A.21) M_{Min}	smaller of the two solutions above
(Eq. A.22) M_{Ave}	average of the two solutions above
(Eq. A.23) $M_{\text{BothSolutions}}$	each of two solutions above is given weight $\frac{1}{2}$

TABLE XI: The $W\gamma$ system mass estimators are tabulated.

average value

$$M_{\text{Ave}} = \frac{M_{\text{Sol1}} + M_{\text{Sol2}}}{2} \quad (\text{A.22})$$

may be histogrammed or each solution may be included in the histogram with half weight

$$M_{\text{BothSolutions}} : \text{ histogram } M_{\text{Sol1}}, M_{\text{Sol2}} \text{ each with weight } \frac{1}{2}. \quad (\text{A.23})$$

The cluster transverse mass is a directly observable estimator which does not rely on the assumptions of Eqs. A.18 and A.19,

$$M_{\text{Tran}}(l_W^\pm\gamma; P_{\text{miss}}^T) = \sqrt{\left(\sqrt{M^{\text{inv}}(l_W^\pm\gamma)^2 + |\vec{P}_\gamma^T + \vec{P}_{l_W^\pm}^T|^2 + P_{\text{miss}}^T}\right)^2 - \left|\vec{P}_\gamma^T + \vec{P}_{l_W^\pm}^T + \vec{P}_{\text{miss}}^T\right|^2} \quad (\text{A.24})$$

where $M^{\text{inv}}(l_W^\pm\gamma)$ is the invariant mass of the l_W^\pm, γ system. The M_{Tran} estimator represents the minimum invariant mass of the $\gamma, l_W^\pm, \vec{P}_{\text{miss}}^T$ cluster, and so it is always smaller than M_{Truth} .

For the convenience of the reader, the various definitions of the $W\gamma$ system mass estimators are enumerated in Table XI.

In order to evaluate the effectiveness of the estimators, the mass difference $M_{\text{Truth}} - M_{\text{Reconstructed}}$ distributions, where $M_{\text{Reconstructed}}$ is any of the estimators of Table XI, are shown in Figure 17. A non-zero mean indicates a bias, whereas the root-mean-square is an indicator of the estimator resolution. The distributions for high P_γ^T events have been checked and are similar to what is presented in Figure 17.

The $M_{\text{WrongSolution}}$ resolution represents the case where the incorrect mass is chosen every time, and so reflects the worse case situation when the mass is reconstructed using the assumptions of Eqs. A.18 and A.19. Whenever the true mass is the larger of the two solutions, M_{Min}

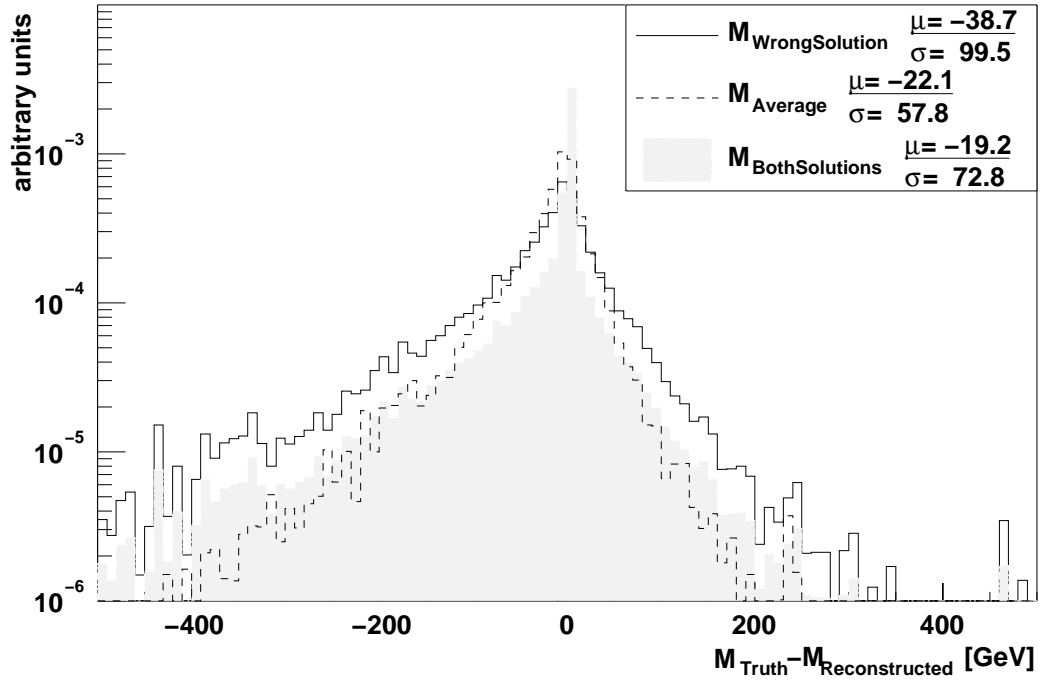
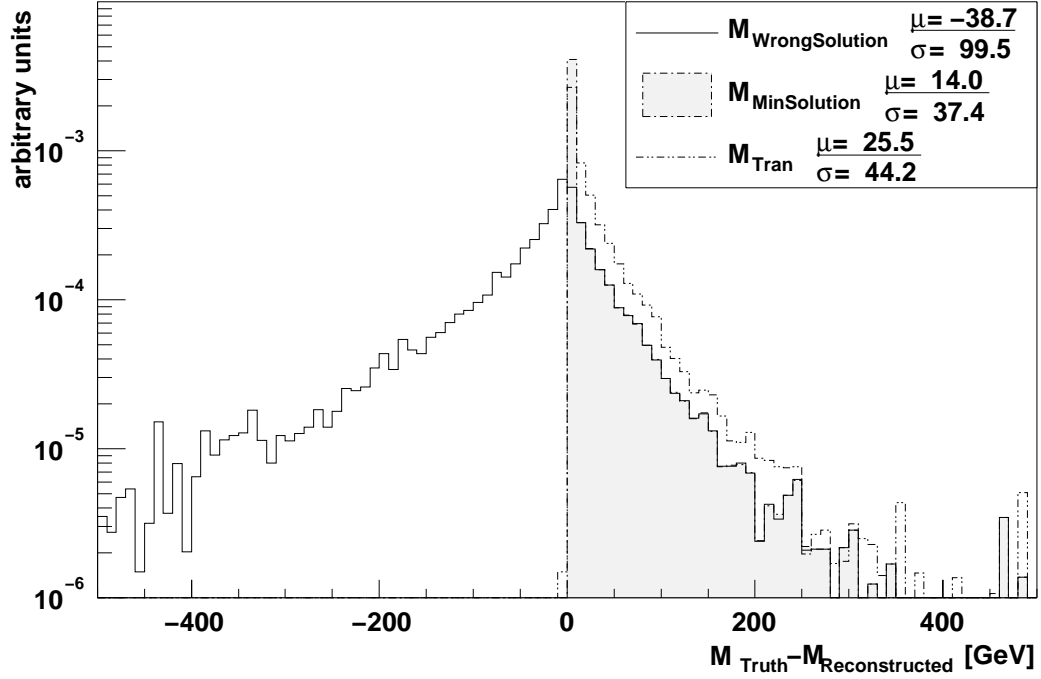


FIG. 17: The mass difference for the $W\gamma$ system invariant mass estimators of Table XI are shown. The mean and root-mean-square (μ and σ , in GeV) of each distribution are printed in the legend. The event sample is $pp \rightarrow W^+(\rightarrow l^\pm\nu)\gamma$ generated using the BHO NLO generator at the parton level with no detector smearing or backgrounds.

corresponds precisely to $M_{\text{WrongSolution}}$, and so the two distributions coincide in the positive resolution region. Being the minimum solution, M_{Min} is biased towards small mass values. The average mass M_{Ave} is biased towards large reconstructed mass values because the relative probability of the larger mass solution is usually considerably smaller than for the small mass solution. In the positive mass resolution region of Figure 17, the transverse mass M_{Tran} resolution is considerably worse than the $M_{\text{WrongSolution}}$ or M_{Min} resolutions. The $M_{\text{BothSolutions}}$ distribution appears narrower than any other in the central region of Figure 17, but suffers from long tails, resulting in a large root-mean-square.

The best resolution is obtained from the M_{Min} estimator, which has a root-mean-square of about 35 GeV. This estimator is biased, but the bias is similar or smaller than the biases from other estimators. As such, M_{Min} is a good choice for evaluating the $W\gamma$ system mass.